

Discrete event simulations for glycolysis pathway and energy balance

Citation for published version (APA):

Zwieten, van, D. A. J., Rooda, J. E., Armbruster, H. D., & Nagy, J. D. (2010). *Discrete event simulations for glycolysis pathway and energy balance*. (SE report; Vol. 2010-02). Technische Universiteit Eindhoven.

Document status and date:

Published: 01/01/2010

Document Version:

Publisher's PDF, also known as Version of Record (includes final page, issue and volume numbers)

Please check the document version of this publication:

- A submitted manuscript is the version of the article upon submission and before peer-review. There can be important differences between the submitted version and the official published version of record. People interested in the research are advised to contact the author for the final version of the publication, or visit the DOI to the publisher's website.
- The final author version and the galley proof are versions of the publication after peer review.
- The final published version features the final layout of the paper including the volume, issue and page numbers.

[Link to publication](#)

General rights

Copyright and moral rights for the publications made accessible in the public portal are retained by the authors and/or other copyright owners and it is a condition of accessing publications that users recognise and abide by the legal requirements associated with these rights.

- Users may download and print one copy of any publication from the public portal for the purpose of private study or research.
- You may not further distribute the material or use it for any profit-making activity or commercial gain
- You may freely distribute the URL identifying the publication in the public portal.

If the publication is distributed under the terms of Article 25fa of the Dutch Copyright Act, indicated by the "Taverne" license above, please follow below link for the End User Agreement:

www.tue.nl/taverne

Take down policy

If you believe that this document breaches copyright please contact us at:

openaccess@tue.nl

providing details and we will investigate your claim.

Systems Engineering Group
Department of Mechanical Engineering
Eindhoven University of Technology
PO Box 513
5600 MB Eindhoven
The Netherlands
<http://se.wtb.tue.nl/>

SE Report: Nr. 2010-2

Discrete event simulations for
glycolysis pathway and energy
balance

D.A.J. van Zwieten, J.E. Rooda,
D. Armbruster and J.D. Nagy
April 13, 2010

ISSN: 1872-1567

SE Report: Nr. 2010-2
Eindhoven, April 2010
SE Reports are available via <http://se.wtb.tue.nl/sereports>

Abstract

In this report, the biological network of the glycolysis pathway has been modeled using discrete event models (DEMs). The most important feature of this pathway is that energy is released. To create a stable steady-state system an energy molecule equilibrating enzyme and metabolic reactions have been added, resulting in the energy balance system. Stability and stochastic influences on the results have been investigated and result in an unstable system, except for a small region of input parameters. To stabilize the energy balance system some feedback regulators are presented. It is shown that stochastic behavior has got a significant influence on a otherwise stable biological system.

Contents

1	Introduction	5
2	Glycolysis	7
3	ODE approach	9
3.1	Simulation results	11
4	Manufacturing approach	15
4.1	Simulation results	16
4.2	Including feedback	19
4.3	Stochastic behavior	21
4.4	Steady-state analysis	24
4.5	Molecule concentration analysis	27
5	Adenylate transitions	31
5.1	Energy charge	33
5.2	Stability	34
5.3	Conclusion	38
6	Energy balance regulation	41
6.1	Regulation by energy charge	41
6.2	Molecule concentration analysis	49
6.3	Regulation by <i>AMPK</i>	52
6.4	Regulation: $2\lambda - \mu_1 - 2\mu_2 = 0$	58
6.5	Continuous regulator	60
6.6	Conclusions	62
7	Conclusions and recommendations	63
	Bibliography	65
A	Parameters	67
B	Chi processes	69
B.1	Enzymes	69
B.2	Metabolism	72
B.3	Buffers	72
C	Chi models	75
C.1	Glycolysis pathway	75
C.2	Adenylate transitions	78

Chapter 1

Introduction

Why does the functioning of biological systems seem miraculous? One reason is that we do not know how to design systems that do what cells do. In contrast, we know how to design highly complex information systems. The fundamental reason for the successful evolution of information systems is the development of mathematical abstractions that enable efficient and robust design processes. In the physical sciences and engineering, mathematical models are usually expressed in terms of nearly exactly measurable quantities and the goal is to obtain precise quantitative results to be compared with experimental observations. In the biological sciences however, it is rare that the phenomenon to be studied can be so precisely quantified, due to the complexity of the systems to be considered. It is difficult to account for all the intricacies of predator-prey interactions, tumor growth or the spread of infectious diseases for example. Typically biological models are more qualitative, aiming to predict only quantitative features rather than yielding detailed quantitative results.

Applying mathematics to biology has a long history, but only recently there has been an explosion of interest in the field. Some reasons for this include a better understanding of how molecules and cells function due to continued development and innovations in experimental and visualizing tools. Examples are Fluorescence Correlation Spectroscopy and Nuclear Magnetic Resonance where systems can be investigated on a molecular level. These techniques renewed the interest in biological networks with a small number of molecules, and therefore modeling these networks is important for new insights. Also development of mathematical tools and an increase in computing power enabled performing calculations and simulations that were not previously possible. Another contribution is an increasing interest in *in silico* experimentation, i.e. via computer simulation, due to ethical considerations, risk, unreliability and other complications involved in human and animal research.

This report presents an approach to modeling a biological network consisting of substrate-enzyme reactions as discrete event models (DEMs), which are mostly used in manufacturing and queueing systems. Different types of biological networks exist, e.g. metabolic or signal transduction networks. A biological network consists of a network of chemical substrate-enzyme reactions. *Enzymes* are the proteins that catalyze chemical reactions. In enzymatic reactions, the molecules at the beginning of the process are called *substrate* molecules, and the enzyme reconfigures them into different molecules, called *product*

molecules. With this approach the glycolysis pathway, one of the most ancient and well-studied pathways, has been modeled and studied. In [12], a beginning in modeling the first steps of the glycolysis pathway as a DEM has been described. These first steps have been remodeled and extended with activating and/or inhibiting feedback and reversibility in [14].

In this report the model of [14] has been extended to the complete glycolysis pathway with related energy balancing reactions and enzymes. The glycolysis pathway is presented in Chapter 2 and Chapter 3 presents the ODE model of this pathway, giving some insight in the model. Chapter 4 introduces the DEM of this pathway, based on a manufacturing line approach. The DEM is validated by the ODE model. This chapter also contains analysis of stochastic influence and steady-state behavior. The glycolysis pathway has been extended with metabolic reactions and an energy-molecule equilibrating enzyme in Chapter 5, to keep the energy molecules in the desired balance. This system resulted stable for a very specific relation of input parameters and only in a deterministic setting. Stabilization of the energy balance system with different feedback regulators is presented in Chapter 6. Conclusions and recommendations are given in Chapter 7.

Chapter 2

Glycolysis

In 1860 Louis Pasteur discovered that microorganisms are responsible for fermentation [5]. This led to a new insight and many biological discoveries in the years that followed. The details of the glycolysis pathway were eventually determined in 1940 by Otto Meyerhof and Gustav Embden [9]. This pathway is thought to be the archetype of an universal metabolic pathway. It occurs, with variations, in nearly all organisms and is therefore intensively studied.

The constant supply of energy that cells need to generate and maintain the biological order that keeps them alive comes from the energy in food molecules, which thereby serve as fuel for cells [1]. The major process for converting glucose *Gluc* (sugar) to energy is the sequence of reactions known as glycolysis (from the Greek *glukus*, "sweet" and *lisis*, "rupture"). A scheme of the glycolysis pathway used in this report is presented in Figure 2.1. Glycolysis occurs in the cytosol, the liquid found inside cells, without involvement of oxygen. The high energy molecule considered is adenosine triphosphate *ATP*, which is a convenient and versatile store of energy used to drive a variety of chemical reactions in cells. When required, *ATP* gives up its energy packet and becomes adenosine diphosphate *ADP*. In glycolysis, for each *Gluc* molecule, two molecules of *ATP* are used to provide energy to drive the early steps (reactions denoted by 1 and 3), but four molecules of *ATP* are produced in the later steps by the reactions denoted by 6 and 9. At the end of glycolysis, there is consequently a net gain of two molecules of *ATP* for each broken down *Gluc* molecule. For a layman in the biological world, to get more information about the glycolysis pathway and the molecules involved, you can take a look at [13]. Molecules *ATP*, *ADP*, *NADH* and *NAD*⁺ all are energy carriers and from now on are referred to as 'energy molecules'.

As a starting point the pathway model of [11] has been used. It is argued that applying results from test-tube measures on the enzymes does not always provide a satisfactory understanding of what is happening in cells. Since test-tube measures are used, all reactions are reversible. It is widely thought that most reactions of glycolysis, while technically reversible, are thermodynamically irreversible, i.e. the 'backwards' reaction is thermodynamically unfavorable within a cell and therefore of negligible consequence. Reactions in enzymes *PGI* and *PGM* are assumed reversible since the backward flux can not be neglected.

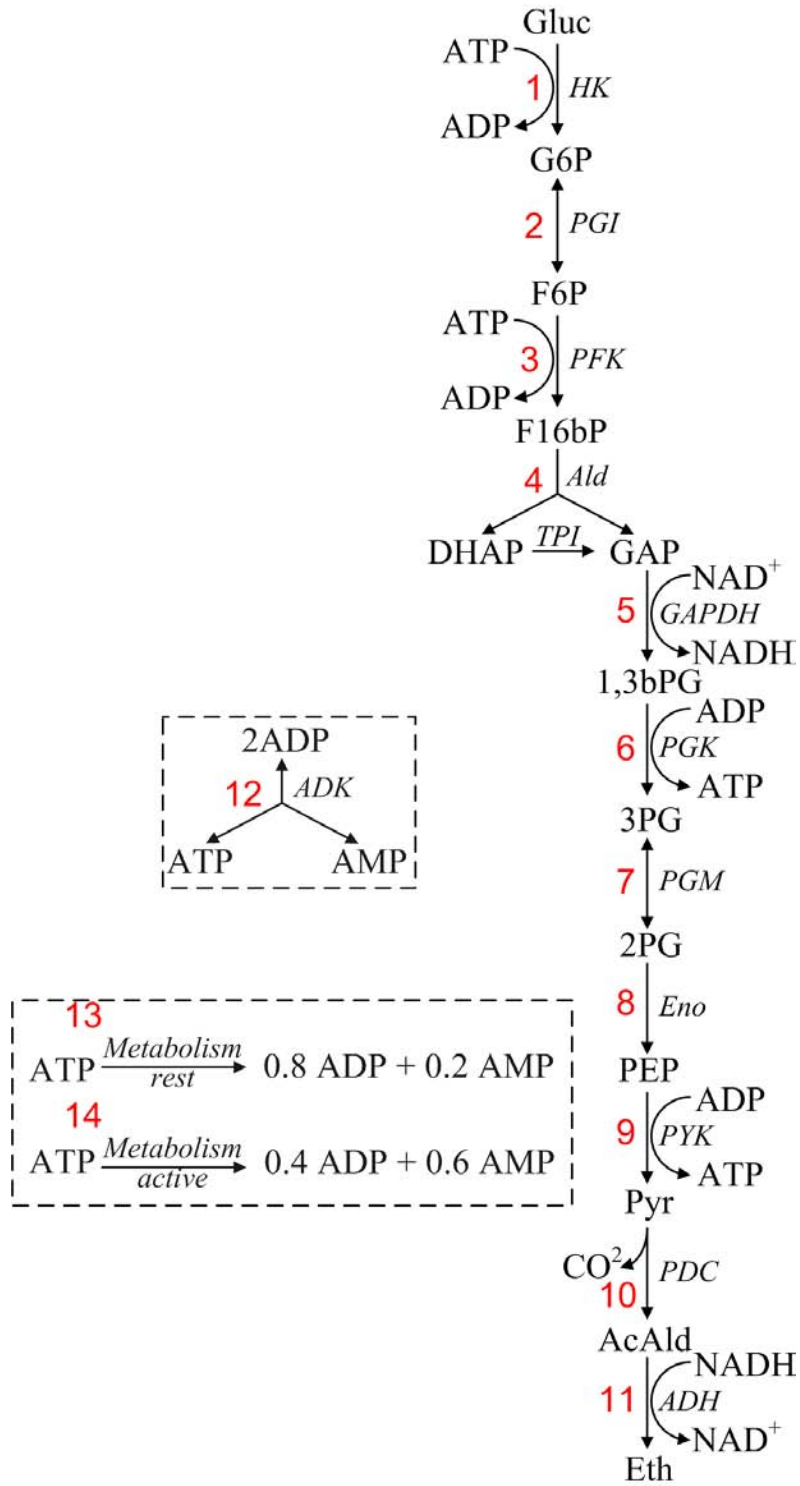


Figure 2.1: Glycolysis reaction scheme with metabolic reactions and equilibrating enzyme ADK.

Chapter 3

ODE approach

In this chapter a set of ordinary differential equations (ODEs) for the glycolysis pathway and simulations with this model are presented. It is assumed that all enzymic reactions in the pathway can be divided into three groups, from [8]:

- Single substrate reactions: A single substrate molecule is reconfigured into a product molecule. Specific activity for this reaction is presented in (3.1a) with maximal reconfiguration rate V_{\max} , Michaelis Menten constant $K_{m,S}$ and substrate concentration C_S .

$$v_S = \frac{V_{\max} C_S}{K_{m,S} + C_S} \quad (3.1a)$$

- Bi-substrate reactions: Two different substrate molecules are reconfigured into two different product molecules. Specific activity is presented in (3.1b) with Michaelis Menten constants for both substrates and the concentration of both substrates.

$$v_{2S} = \frac{V_{\max} \cdot C_{S_1} \cdot C_{S_2}}{\left(K_{m,S_1} + C_{S_1}\right) \cdot \left(K_{m,S_2} + C_{S_2}\right)} \quad (3.1b)$$

- Reversible reactions: Single substrate reaction where a substrate molecule is reconfigured into a product molecule and a product molecule can be reconfigured into a substrate molecule. Specific activity is presented in (3.1c) with equilibrium constant K_{eq} .

$$v_{\text{rev}} = \frac{V_{\max} \cdot \left(C_S - \frac{C_P}{K_{\text{eq}}}\right)}{K_{m,S} \cdot \left(1 + \frac{C_P}{K_{m,P}}\right) + C_S} \quad (3.1c)$$

The ODE model consists of these three enzyme types. In the glycolysis pathway reactions with enzymes *Ald*, *TPI*, *Eno* and *PDC* are single substrate reactions, reactions with enzymes *HK*, *PFK*, *GAPDH*, *PGK*, *PYK* and *ADH* are bi-substrate reactions and reactions with enzymes *PGI* and *PGM* are considered reversible. With specific activities defined in (3.1) and the pathway described in Figure 2.1, the set of ODEs belonging to

this pathway is:

$$\frac{dGluc}{dt} = -v_{HK}, \quad (3.2a)$$

$$\frac{dG6P}{dt} = v_{HK} - v_{PGI}, \quad (3.2b)$$

$$\frac{dF6P}{dt} = v_{PGI} - v_{PFK}, \quad (3.2c)$$

$$\frac{dF1,6bP}{dt} = v_{PFK} - v_{Ald}, \quad (3.2d)$$

$$\frac{dDHAP}{dt} = v_{Ald} - v_{TPI}, \quad (3.2e)$$

$$\frac{dGAP}{dt} = v_{Ald} + v_{TPI} - v_{GAPDH}, \quad (3.2f)$$

$$\frac{d1,3bPG}{dt} = v_{GAPDH} - v_{PGK}, \quad (3.2g)$$

$$\frac{d3PG}{dt} = v_{PGK} - v_{PGM}, \quad (3.2h)$$

$$\frac{d2PG}{dt} = v_{PGM} - v_{Eno}, \quad (3.2i)$$

$$\frac{dPEP}{dt} = v_{Eno} - v_{PYK}, \quad (3.2j)$$

$$\frac{dPyr}{dt} = v_{PYK} - v_{PDC}, \quad (3.2k)$$

$$\frac{dCO_2}{dt} = v_{PDC}, \quad (3.2l)$$

$$\frac{dAcAld}{dt} = v_{PDC} - v_{ADH}, \quad (3.2m)$$

$$\frac{dEth}{dt} = v_{ADH}, \quad (3.2n)$$

$$\frac{dNADH}{dt} = v_{GAPDH} - v_{ADH}, \quad (3.2o)$$

$$\frac{dNAD^+}{dt} = v_{ADH} - v_{GAPDH}, \quad (3.2p)$$

$$\frac{dATP}{dt} = -v_{HK} - v_{PFK} + v_{PGK} + v_{PYK}, \quad (3.2q)$$

$$\frac{dADP}{dt} = v_{HK} + v_{PFK} - v_{PGK} - v_{PYK}. \quad (3.2r)$$

Scaled parameters for all reactions are presented in Appendix A. These parameters are derived from [11]. It is assumed that the mass of each enzyme in the system is equal to 1mg. This corresponds to about 10-40 nMol per enzyme, and is therefore much smaller than the substrate concentrations.

For an infinite number of substrate molecules enzyme *PGM* reconfigures substrates at the highest rate, 1.0 mMol per minute, and enzyme *PDC* reconfigures substrates at the lowest rate, 0.069 mMol per minute.

3.1 Simulation results

With the set of ODEs, simulations can be performed depending on the initial concentrations. For an initial concentration of 5 mMol for each energy molecule and 3 mMol for the other concentrations (except CO_2 and Eth), simulation results are presented in Figures 3.1, 3.2 and 3.3. The results show a quick depletion of ADP . This slows down enzymes PGK and PYK leading to a build-up in concentration of $1,3bPG$ and PEP . Figure 3.2 shows an increase of GAP after 20 time units, since the NAD^+ concentration is zero, this shows the importance of fermentation, it regenerates NAD^+ depending on the GAP concentration to prevent high concentrations of GAP in the cell.

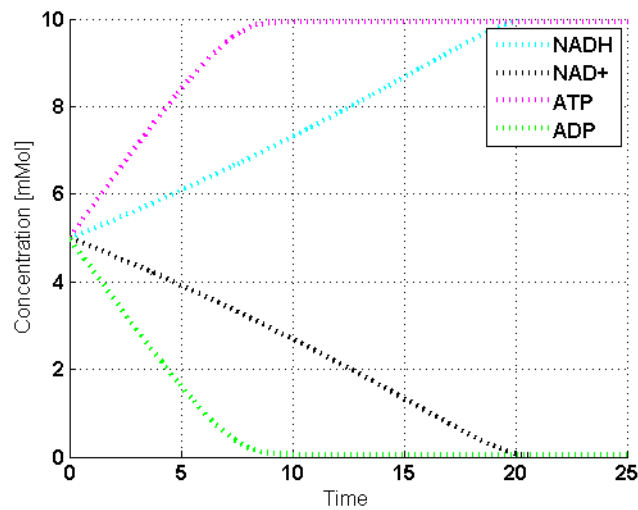


Figure 3.1: ODE simulation results: Energy molecule concentrations

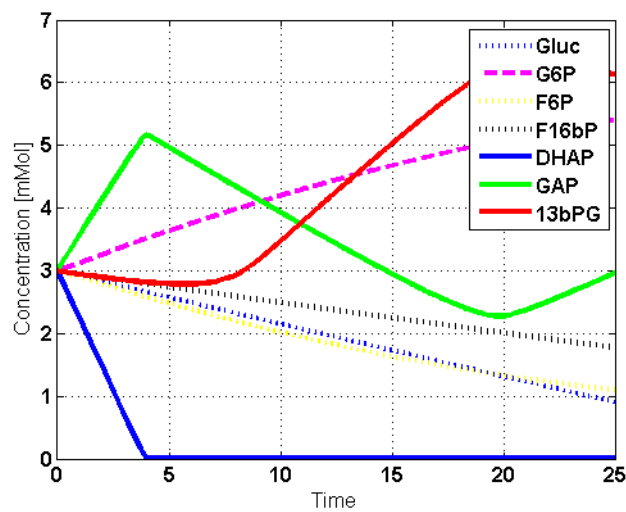


Figure 3.2: ODE simulation results: concentrations of *Gluc* - *13bPG*

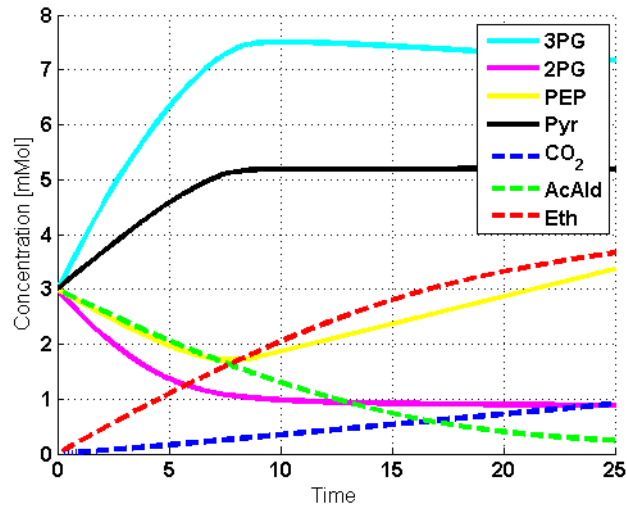


Figure 3.3: ODE simulation results: concentrations of 3PG - Eth

Another transient simulation is with an initial *Gluc* concentration $C_{\text{Gluc}}(0) = 6\text{mMol}$, the energy molecule initial concentrations are 5mMol and all non-energy molecule initial concentrations are 0 mMol. Results of this simulation are presented in Figures 3.4, 3.5 and 3.6. It can be seen that C_{NAD^+} depletes since all molecules first react with enzyme *GAP*. C_{ADP} shows a little increase before depleting since it takes time for the *ADP*-consuming enzymes *PGK* and *PYK* to bind with their substrate molecules. The C_{G6P} shows a peak due to the depletion of C_{Gluc} , C_{GAP} builds up when C_{NAD^+} depletes and C_{13bPG} builds up when C_{ADP} depletes. C_{Pyr} , C_{3PG} and C_{PEP} are also affected by the depletion of one of the energy molecules, since they are required for their reaction. Formation of C_{Eth} , however, shows no effects of the upstream fluctuations. This can be explained by the fact that enzyme *PDC* is very slow compared to the rest of the system.

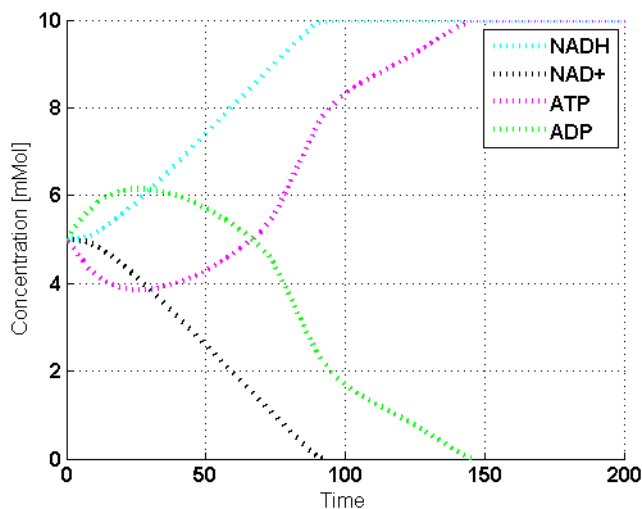


Figure 3.4: ODE simulation results: Energy molecule concentrations

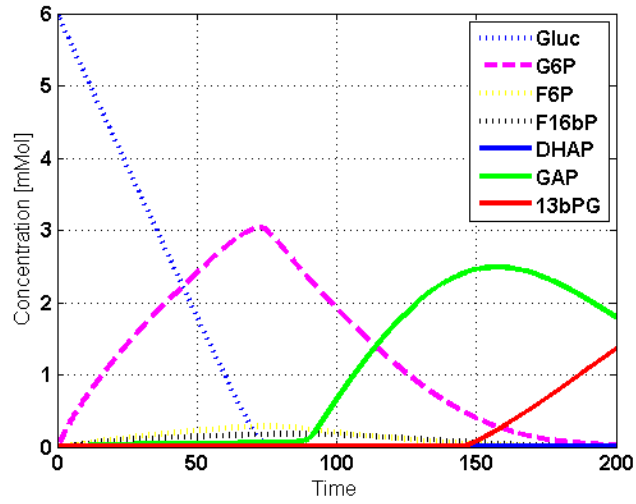


Figure 3.5: ODE simulation results: concentrations of *Gluc* - *13bPG*

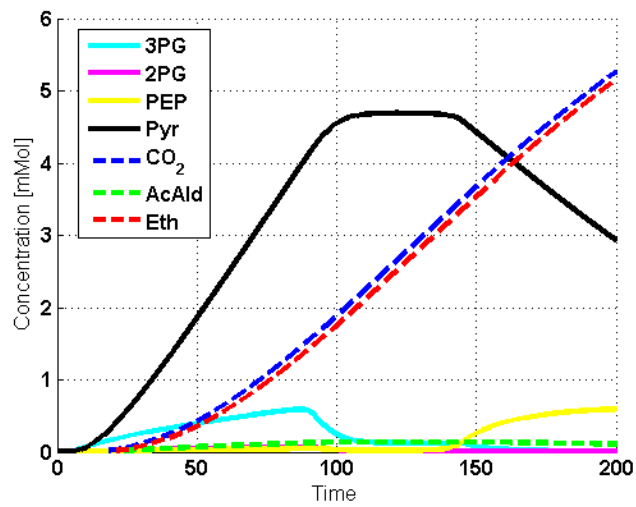


Figure 3.6: ODE simulation results: concentrations of *3PG* - *Eth*

Chapter 4

Manufacturing approach

In the manufacturing approach a distinction has been made between two processes; search process and reconfiguration process. In the search process an enzyme waits a certain search time τ_s (4.2) before a substrate molecule binds; this represents the time it takes for an enzyme and a substrate molecule to collide in the cell. When a substrate is bound, i.e. begin of the reconfiguration process, the enzyme reconfigures the substrate molecule into a product molecule. This reconfiguration time is denoted by τ_r (4.1).

$$\tau_r = \frac{1}{V_{\max} \cdot V}, \quad (4.1)$$

with volume of the cell V and maximal reaction rate V_{\max} ,

$$\tau_s = \frac{K_m}{C_S} \cdot \tau_r, \quad (4.2)$$

with Michealis-Menten constant K_m and substrate concentration C_S .

In [14] the first steps of the pathway has been constructed out of multiple processes and functions. The DEM of the glycolysis pathway is constructed in a similar way and a representation of the DEM is presented in Figure 4.1. Rectangular blocks represent buffers with molecules and reaction processes catalyzed by enzymes are denoted by circles. The lines show the path of the molecules. Intersected lines represent energy molecule channels. Outgoing channels of enzymes *PGK* and *PYK* lead to buffer *ATP* (dotted lines). The model has been build from existing processes and functions from [14] and new processes presented in Appendix B. The complete model with all channels is presented in Appendix C. A simplification of the DEM representation of the glycolysis pathway is presented in Figure 4.2. The *ADP* and *ATP* buffers are not included in the glycolysis box since they play an important role in the energy transitions in Chapter 5.

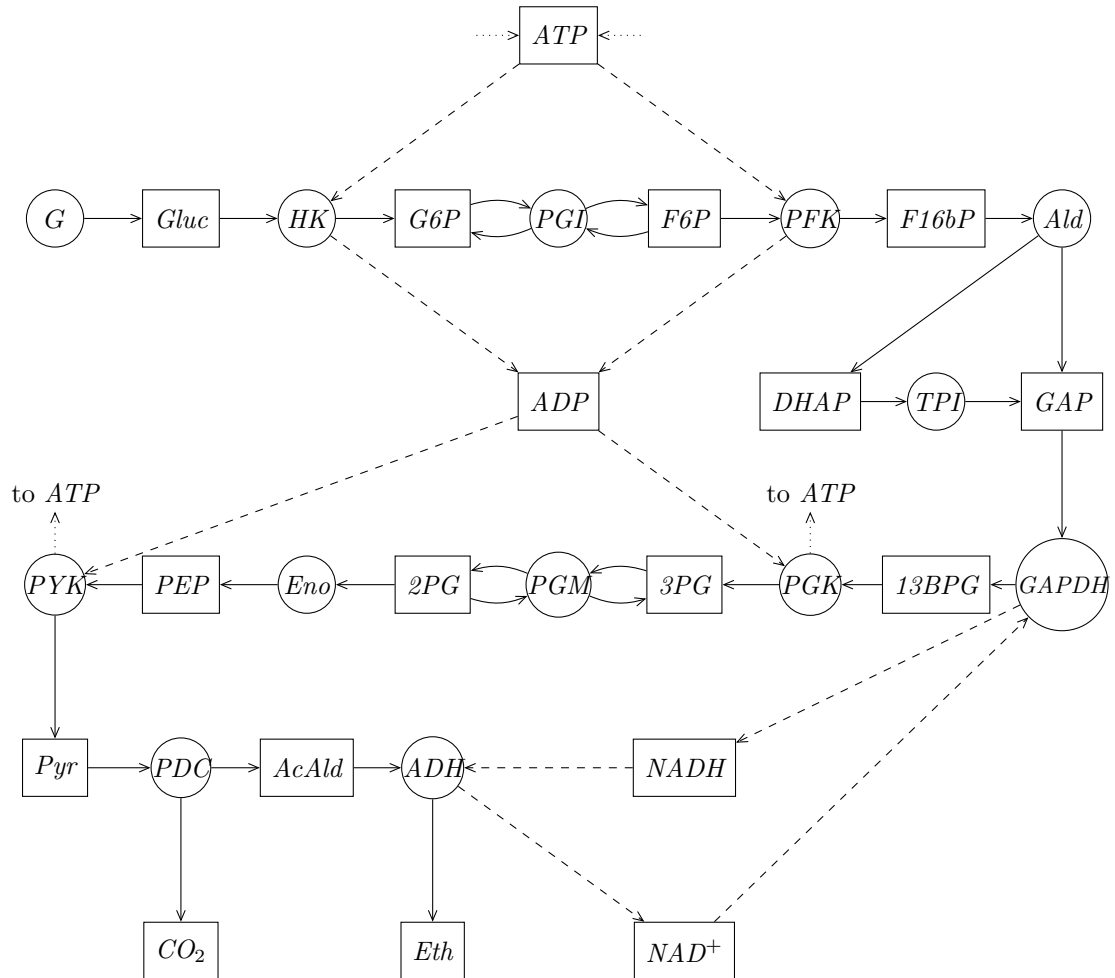


Figure 4.1: DEM representation of the glycolysis pathway.

4.1 Simulation results

Simulations with a transient system have been performed first to check if the results match the ODE results. This implies generator G does not generate any new molecules. An initial concentration of 5 mMol for each energy molecule and 3 mMol for the other concentrations (except CO_2 and Eth) has been taken and parameters used are shown in Appendix A. The simulation results of the DEM are presented in Figures 4.3, 4.4 and 4.5. The first figure shows all energy molecule concentrations, while the other figures show the remaining concentrations. It can be seen that the DEM results match the ODE results as expected. This concludes that the DEM has been constructed properly.

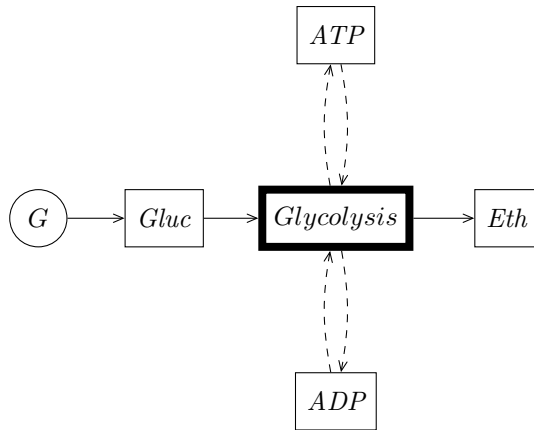


Figure 4.2: Compact representation of the glycolysis pathway.

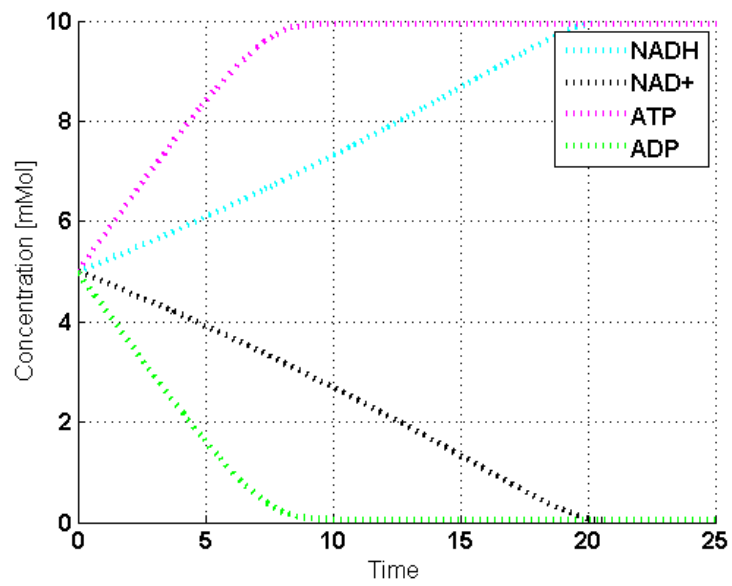


Figure 4.3: DEM simulation results: Energy molecule concentrations

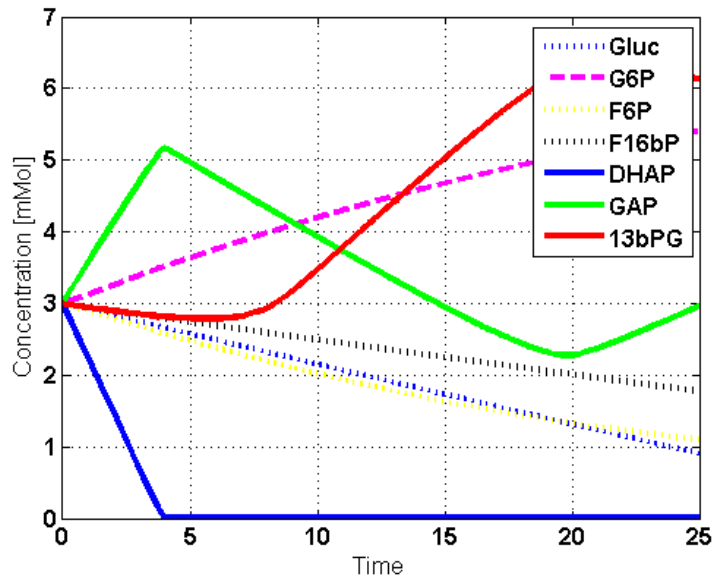


Figure 4.4: DEM simulation results: concentrations of *Gluc* - *13bPG*

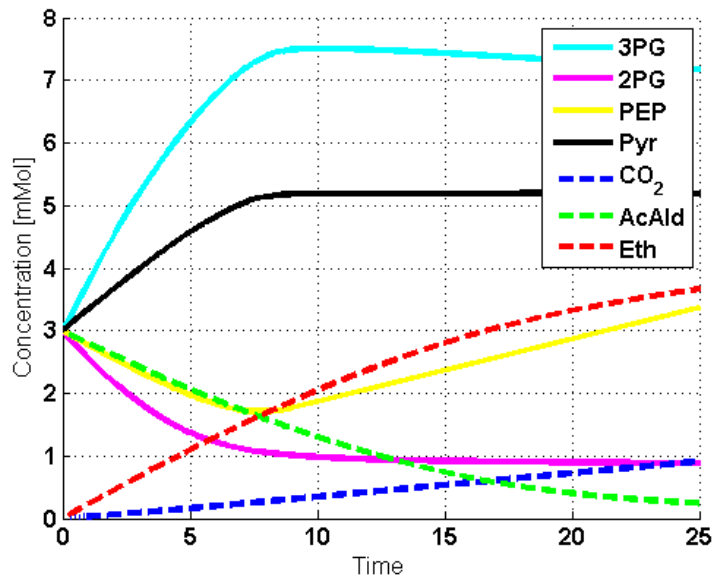


Figure 4.5: DEM simulation results: concentrations of *3PG* - *Eth*

4.2 Including feedback

It is believed that the main feedback in the glycolysis pathway occurs at enzyme *PFK*. This enzyme is inhibited by *ATP* and activated by *ADP*. So, the enzyme contains two different catalytic sites (*F6P* and *ATP*) and one regulatory site that can bind either *ATP* or *ADP*. Also enzymes *HK* and *GAPDH* are under regulatory feedback. The upstream energy molecules (*ATP* for enzymes *HK* and *PFK* and *NAD⁺* for enzyme *GAPDH*) inhibit the enzyme and downstream energy molecules (*ADP* for enzymes *HK* and *PFK* and *NADH* for enzyme *GAPDH*) activate the enzyme. All regulatory feedback is assumed to affect the search process. Further details on regulatory feedback is presented in [14]. If the regulatory site binds with an activating molecule, the search process is accelerated by a factor of 50. If an inhibiting feedback molecule binds the search process will be paused until the feedback molecule unbinds. Feedback binding time is assumed to be 1 second. The simulation results of the energy concentrations in the system are presented in Figure 4.6. *ADP* and *ATP* concentrations are almost similar to the results of the system without feedback, while the concentrations of *NADH* and *NAD⁺* differ a lot. This argues that the main feedback occurs in enzyme *GAPDH* instead of enzyme *PFK*. Figure 4.7 presents the first part of the non-energy molecule concentrations. Compared to the results of the system without feedback in Figure 4.4, the concentrations of *GADP* and *1,3bPG* differ a lot. This is because of the feedback on enzyme *GAPDH*. The feedback has very little effect on downstream products, see Figure 4.8.

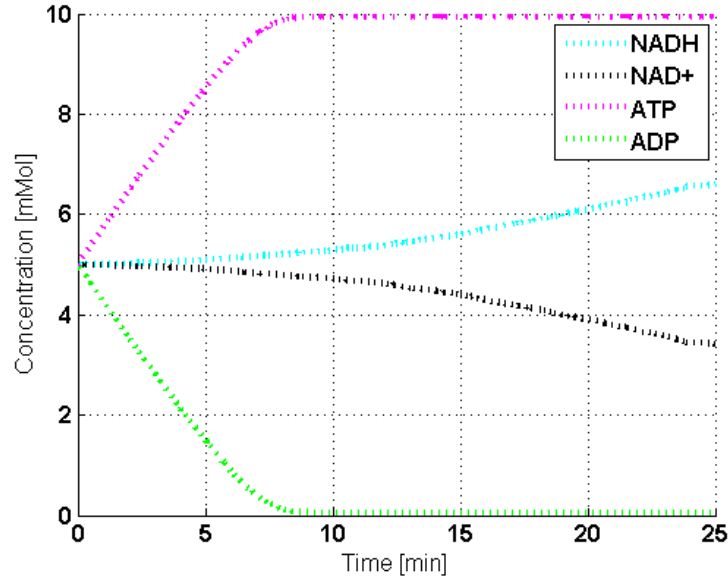


Figure 4.6: DEM Feedback simulation results: Energy molecule concentrations

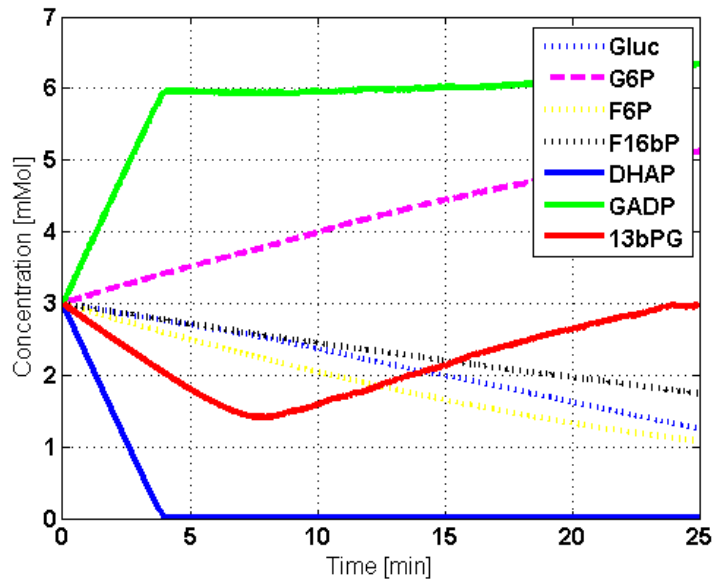


Figure 4.7: DEM Feedback simulation results: concentrations of *Gluc* - *13bPG*

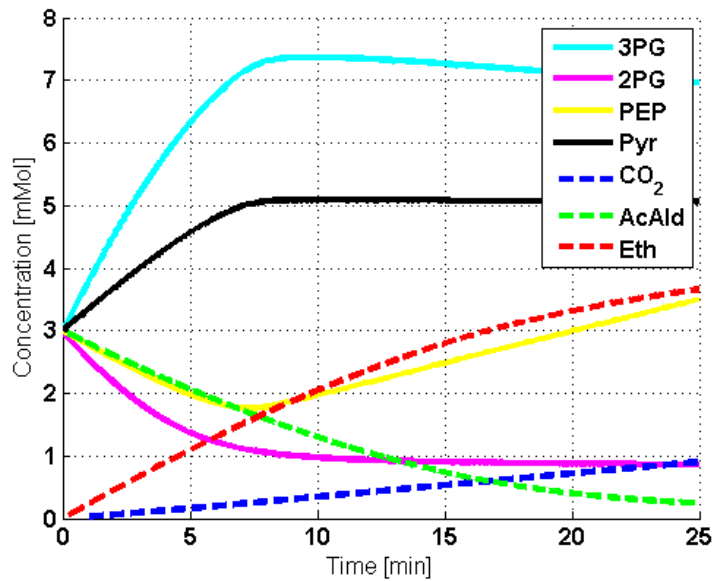


Figure 4.8: DEM Feedback simulation results: concentrations of *3PG* - *Eth*

4.3 Stochastic behavior

The effect of stochastic behavior on the transient system is researched in this section. The search process is considered exponentially distributed. Reconfiguration time is assumed to be Γ distributed with a coefficient of variation (CV) of 3.0. A more detailed description of the stochastic distributions can be found in [14].

A comparison of the final product of the glycolysis pathway, *Eth*, with the deterministic and stochastic model is presented in Figure 4.9. In this figure the deterministic result (red dotted line) and results of five stochastic simulations are shown (blue lines). Initial concentrations are; *Gluc* = 1.0mMol, *ATP* = 1.0mMol, *ADP* = 2.0mMol, *NADH* = 0.5mMol, *NAD*⁺ = 0.5mMol and all other initial concentrations are equal to zero. The stochastic results do not differ much from the deterministic results in this case.

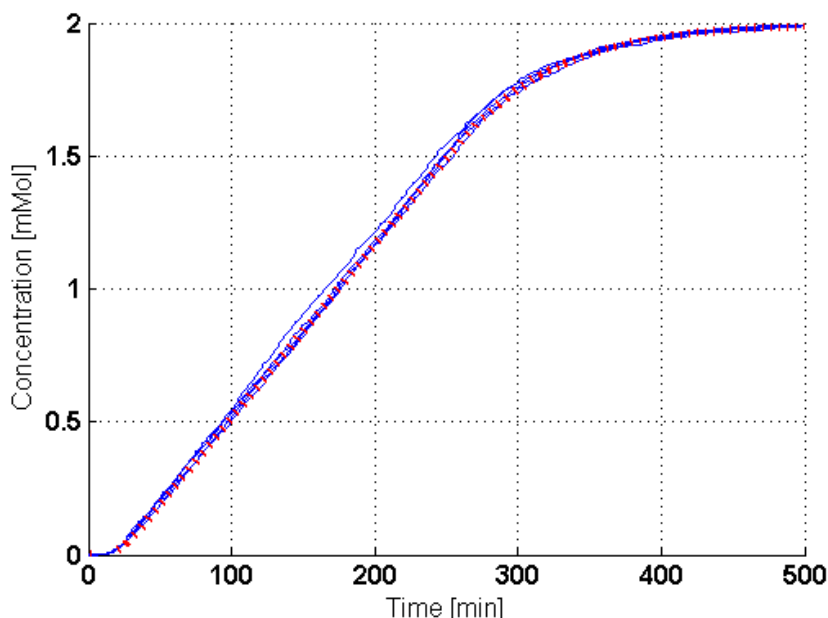


Figure 4.9: Comparison of *Eth* concentration, deterministic (red dotted) and stochastic (blue lines) results

In the previous case, stochastic distributions didn't influence the systems behavior much. It is expected that with few molecules in the cell the stochastic differences are significant. Results of transient stochastic simulations are presented in Table 6.1. This table shows the clearing time of a transient glycolysis pathway without reversible reactions and constant *ATP*, *ADP*, *NAD*⁺ and *NADH* buffers. For the stochastic values, results of 15000 simulations are used. It can be seen that the coefficient of variation decreases if there are more molecules in the system, this is also presented in Figure 4.10.

The difference between the mean stochastic and deterministic clearance times are very small, see Figure 4.11. This is not expected comparing this system to a manufacturing line of 12 machines with buffers in between, described in [10]. Total search time of all reactions for 1 energy molecule and 1 substrate molecule is 1401 time units. The total reconfiguration time of all reactions is 0.07 time units. It can be seen that $\tau_s \gg \tau_r$ and the reconfiguration time can be neglected for a low number of molecules. Note that the

Table 4.1: Comparison of deterministic and stochastic simulation results.

$[Gluc]_0$	$[Energy]_0$	Deterministic clearing time	Stochastic clearing time	Coefficient of variation	Min	Max	Difference
$[\mu Mol]$	$[\mu Mol]$	$[t]$	$[t]$	$[\%]$	$[t]$	$[t]$	$[\%]$
1.00	1.00	1602.47	1630.77	60.55	141.01	11067.57	1.77
	5.00	387.31	414.77	52.21	54.42	2156.79	7.09
	50.00	141.43	144.29	51.52	19.64	801.91	2.02
2.00	1.00	2036.14	2185.56	51.61	398.25	11021.96	7.34
	5.00	474.25	531.99	44.01	117.04	2577.28	12.18
	50.00	166.05	185.68	42.22	30.72	753.61	11.82
3.00	1.00	2351.16	2535.32	46.66	523.92	11884.89	7.83
	5.00	537.51	600.59	39.62	142.79	2536.64	11.73
	50.00	191.85	207.38	38.11	48.61	781.62	8.09
4.00	1.00	2595.53	2792.23	42.59	608.26	10849.14	7.58
	5.00	585.81	654.24	36.62	182.58	2305.50	11.68
	50.00	210.83	225.75	35.10	60.00	752.52	7.07
5.00	1.00	2844.43	2997.62	40.21	701.22	12977.17	5.39
	5.00	633.52	695.95	35.22	210.35	2743.25	9.85
	50.00	224.60	237.93	32.75	76.62	816.13	5.93
10.00	1.00	3521.58	3669.51	34.01	1110.09	14867.76	4.20
	5.00	771.59	833.07	29.96	306.66	3096.87	7.97
	50.00	271.59	283.29	28.46	118.51	859.64	4.31
20.00	1.00	4306.76	4435.24	28.57	1567.51	13757.90	2.98
	5.00	929.08	990.87	25.80	450.51	3032.61	6.65
	50.00	319.57	328.00	24.61	161.89	902.29	2.64
50.00	1.00	5513.68	5645.86	23.01	2732.11	14414.76	2.40
	5.00	1173.54	1227.34	21.46	625.06	3668.97	4.58
	50.00	383.15	387.71	20.71	207.81	979.52	1.19
100.00	1.00	6704.99	6811.79	19.03	3497.84	14566.72	1.59
	5.00	1412.80	1462.38	17.64	864.88	3629.05	3.51
	50.00	435.21	439.51	18.27	266.74	1137.30	0.99
200.00	1.00	8398.90	8507.91	15.42	5526.11	17426.46	1.30
	5.00	1753.30	1804.02	14.59	1128.16	3334.54	2.89
	50.00	494.89	496.90	16.00	319.16	1106.49	0.41
500.00	1.00	12315.57	12398.00	10.60	9097.76	22326.83	0.67
	5.00	2541.51	2594.46	10.40	1906.16	4079.22	2.08
	50.00	602.13	603.82	13.37	429.90	1096.91	0.28

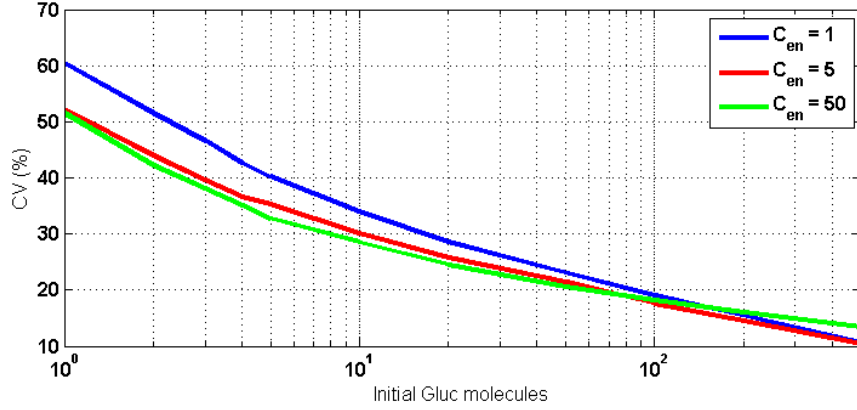


Figure 4.10: Coefficient of variation change by the number of initial *Gluc* molecules.

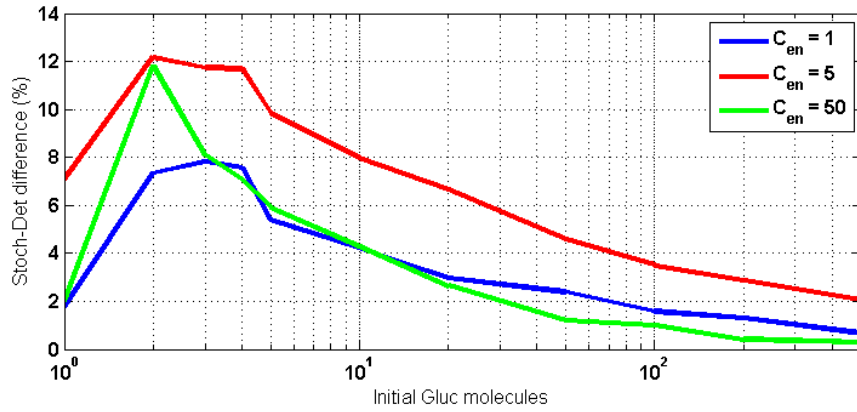


Figure 4.11: Difference between mean stochastic and deterministic simulation results.

sum of total search and reconfiguration time are not equal to the deterministic clearing time presented in Table 6.1 since the calculation is based on a single substrate molecule, where in the glycolysis system 2 substrate molecules are present after the reaction with enzyme *Ald*. For a network of reactions with a single substrate the clearing time τ_{clear} can be calculated by (4.3) and the corresponding coefficient of variation by (4.4). For the single substrate, single energy molecules case the coefficient of variation is 57%.

$$\tau_{\text{clear}} = \sum_{i=1}^n \tau_{s,i}, \quad (4.3)$$

$$CV = \frac{\sqrt{\sum_{i=1}^n \sigma_{s,i}^2}}{\mu_{\tau_{\text{clear}}}}. \quad (4.4)$$

In a line of multiple buffers and machines, e.g. a phone manufacturing line, stochastic fluctuations in arrival and process times causes the clearance time to go up compared to a similar line with deterministic times. This is not the case in this network of substrate-enzyme reactions, as shown in Table 6.1. This difference is caused by the fact that the enzyme is not represented by a single manufacturing machine. The reconfiguration of a molecule consists of 2 processes, search and reconfiguration process. Reconfiguration process can be presented by a machine with a raw process time equal to $1/V_{\text{max}}$. Mean

search process time however, is variable and inversely proportional with the buffer content, see (4.2). Therefore this system can not be compared to a line of manufacturing systems and the difference between deterministic and stochastic clearance times is very small.

4.4 Steady-state analysis

The discrete event model from Figure 4.1 is a transient model. This model stops working when *ATP*, *ADP*, *NAD⁺* or *NADH* has been depleted or all *Gluc* molecules are reconfigured into *Eth* molecules. For analyzing a steady-state simulation the DEM has to be extended with an influx of *Gluc* molecules. Also, the *ADP* concentration has to be replenished since every conversion from *Gluc* to *Eth* produces 2 *ATP* molecules and requires 2 *ADP* molecules. The influx has been modeled by a simple generator *G* that produces new *Gluc* molecules with inter-arrival time t_a . *ADP* molecules have to be regenerated to prevent depletion. This happens outside the glycolysis-pathway and therefore a conversion process *C* has been introduced. This process represents conversion from *ATP* to *ADP* with conversion time t_c .

An important notion for this systems is stability. A manufacturing system is called stable if all buffer levels in the system remain bounded. This definition is commonly used for manufacturing systems, see [4]. Two ingredients are necessary to achieve a stable manufacturing system:

- The system characteristics should meet the product inflow (i.e. is it physically possible to process all incoming products?).
- The production policy must stabilize the system.

For example, a manufacturing system that has enough capacity to process all incoming products, but has a production policy that says to process only all odd numbered products is not stable. On the other hand, a manufacturing system with a production policy that says that all incoming products are to be processed as fast as possible, but with an arrival rate of products that outreaches the production capacity is also unstable.

In case of the glycolysis system, without *ADP* or a larger *Gluc* influx than the enzyme capacity the system becomes *unstable*, i.e. substrate molecules are piling up. When the system is *stable*, all *Gluc* molecules can be converted into *Eth* molecules.

To calculate throughput δ of the system, the number of *Eth* molecules produced are counted in a time interval. To obtain better insight about stability, half of the overall average throughput is scaled to mean input $\frac{1}{t_a}$ and dimensionless variable Δ in (4.5) is introduced. Half of the average throughput is used since for every *Gluc* molecule entering the system, two *Eth* molecules exit the system. If $\Delta = 1$ the input is equal to the output, i.e. all incoming *Gluc* molecules will be reconfigured into *Eth* molecules. In a stable system no buffers blow up, and the outflux is twice the influx. For measurement purposes $\Delta \approx 1$ is assumed to be a stable system.

$$\Delta = \frac{0.5\delta}{1/t_a} = 0.5\delta \cdot t_a. \quad (4.5)$$

Initial concentrations of the steady-state simulations are 0.5 mMol for *ATP*, *ADP*, *NAD⁺* or *NADH* and all other concentrations are 0 mMol. In the simulations no feedback is used. The stability boundary is presented in Figure 4.12.

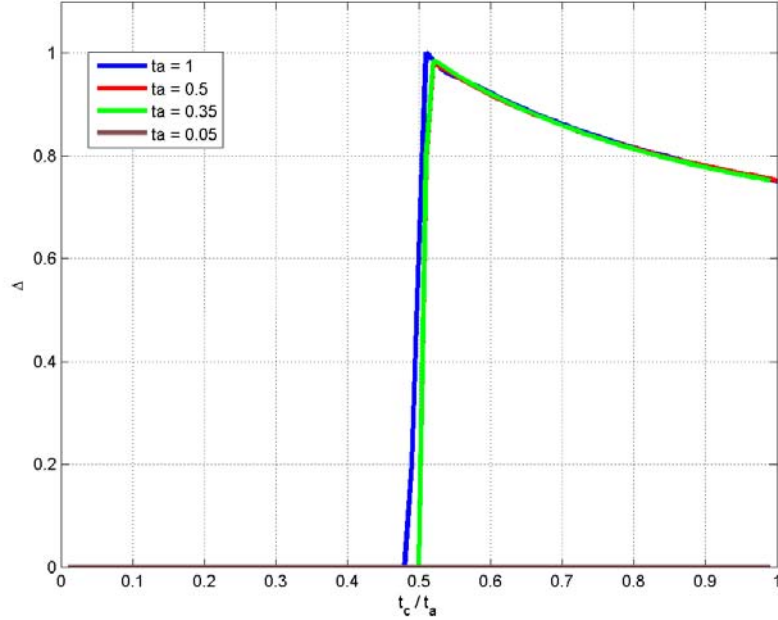


Figure 4.12: Stability boundary.

In the stability boundary figure four regimes can be distinguished:

- *Stable system.* For each *Gluc* molecule entering the system and exiting as *Eth* molecule, two *ATP* molecules are reconfigured into *ADP* molecules and four *ADP* molecules are reconfigured into *ATP* molecules. Therefore, *ADP* regeneration must be twice as fast as the arrival rate to fulfill the need for *ADP*. $t_c/t_a = 0.5$, $\Delta = 1$.
- *Overloaded system due to a high demand for ATP.* If the regeneration is faster than twice the arrival rate, the *ATP* buffer is slowly drained until it is empty and the *Gluc* buffer blows up, see Figure 4.13. This also occurs when glucose influx exceeds the enzymic capacity. Enzyme *PFK* is the bottleneck in this system. If the influx is beyond this enzymes capacity, buffer *ATP* will be depleted by enzyme *HK*. So for $t_c/t_a < 0.5$ and $t_a > t_{enz}$, $\Delta = 0$.
- *Overloaded system due to low demand for ATP.* If the regeneration rate is lower than twice the arrival rate, the *ADP* buffer depletes and buffer *13BPG* grows, see Figure 4.14. There will be a throughput of *Eth* molecules, but it depends on the conversion rate. Therefore, $\Delta < 1$ for $t_c/t_a > 0.5$. If there is no conversion or a very large conversion time and the glucose influx is within the enzyme capacity Δ approaches 0.5.

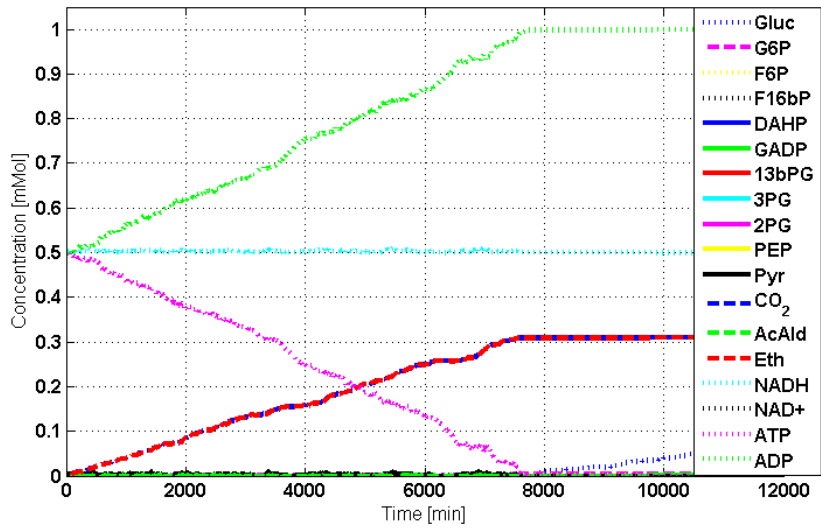


Figure 4.13: $t_a = 0.05$, $t_c = 0.01$: *ATP* demand too high or *Gluc* transport too low for stable system.

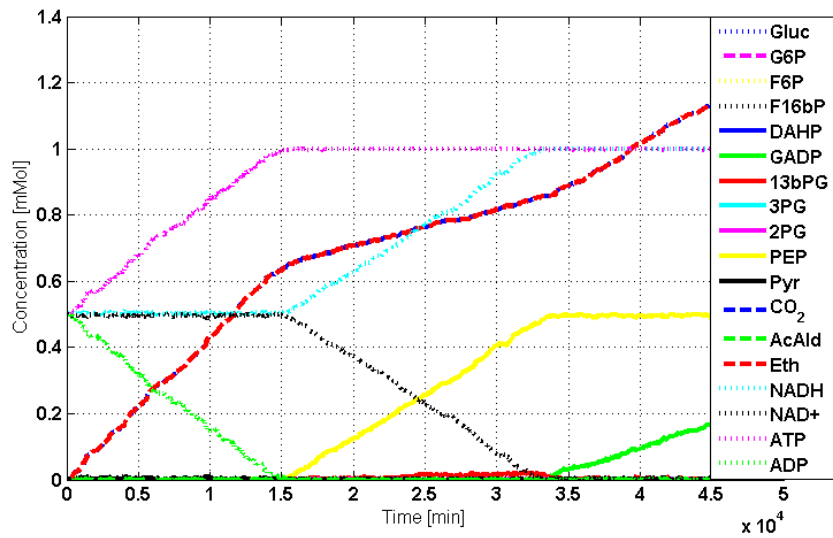


Figure 4.14: $t_a = 0.05$, $t_c = 0.1$: *ATP* demand too low or *Gluc* transport too high for stable system.

4.5 Molecule concentration analysis

The stochastic behavior of a transient system and the stability boundary of the steady-state system have been investigated in the previous sections. To get more information about this system and the stochastic influence, the mean concentration levels of all molecules and the fluctuations of these levels are analyzed in this section.

Initial parameters of all simulations are presented in (4.6) and all initial non-energy concentrations are zero.

$$C_{ATP} = 1000\mu Mol, \quad (4.6a)$$

$$C_{ADP} = 1000\mu Mol, \quad (4.6b)$$

$$C_{NADH} = 500\mu Mol, \quad (4.6c)$$

$$C_{NAD^+} = 500\mu Mol, \quad (4.6d)$$

$$\lambda_G = 12.5\mu Mol/time, \quad (4.6e)$$

$$\mu_C = 25\mu Mol/time. \quad (4.6f)$$

For the glycolysis pathway without reversibility and feedback, mean buffer contents and coefficient of variation of the buffers are presented in Figure 4.15. Figure 4.15a shows the mean value of the energy molecules concentration and the coefficient of variation (CV) of these buffer levels for simulations with the deterministic system. Figure 4.15b presents the mean and CV for simulations with stochastic distributions and Figure 4.15c shows the difference between the deterministic and stochastic results for all buffer levels. The mean buffer levels of the non-energy molecules are not shown since these values are very low (0,5 - 20 μMol), the mean buffer levels of the stochastic and deterministic system are almost similar and compared to the energy molecules the variation can be neglected.

A significant detail in the comparison between results of the system with deterministic and stochastic distributions is the difference in CV for the energy molecule buffer levels. The CV for these levels is 30-90 times higher in the stochastic system. This large fluctuation does not have an effect on the non-energy molecule buffer levels.

Implementing reversible reactions in enzymes *PGI* and *PGM* decreases the fluctuation in the *ATP* and *ADP* buffer levels for the stochastic system, as can be seen in Figure 4.16. Furthermore, there are no significant changes.

With downstream inhibiting and upstream activating feedback from the energy molecules on enzymes *HK*, *PFK* and *GAPDH*, the coefficient of variation for the *ATP* and *ADP* molecules goes up, see Figure 4.17. This drastic increase in CV is not amplified by the stochastic distributions. Note that the deterministic results with feedback are not completely deterministic, as the model for the enzyme with feedback consists of some stochastic distributions, explained in [14].

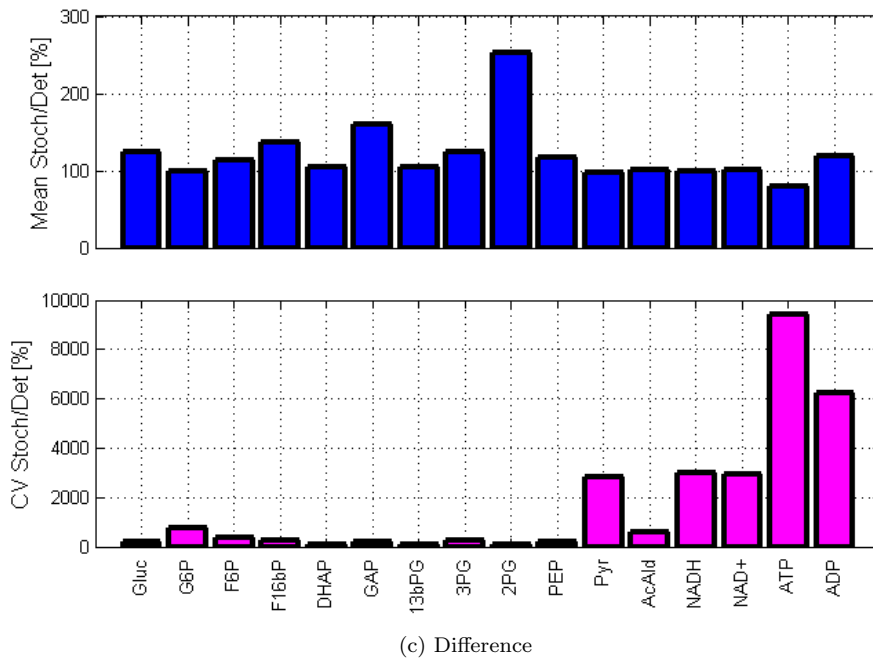
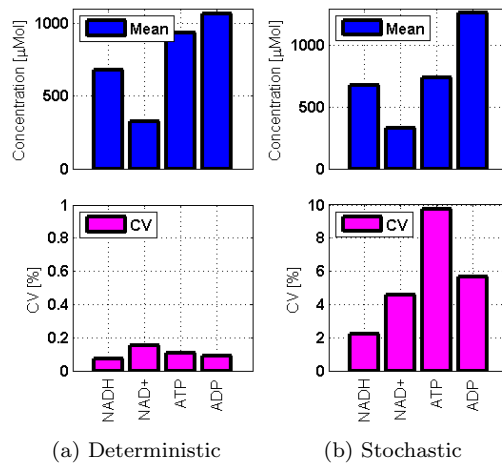


Figure 4.15: Deterministic and stochastic results for the glycolysis system without reversibility, feedback and $\lambda = 0.8$, $\mu_C = 0.4$.

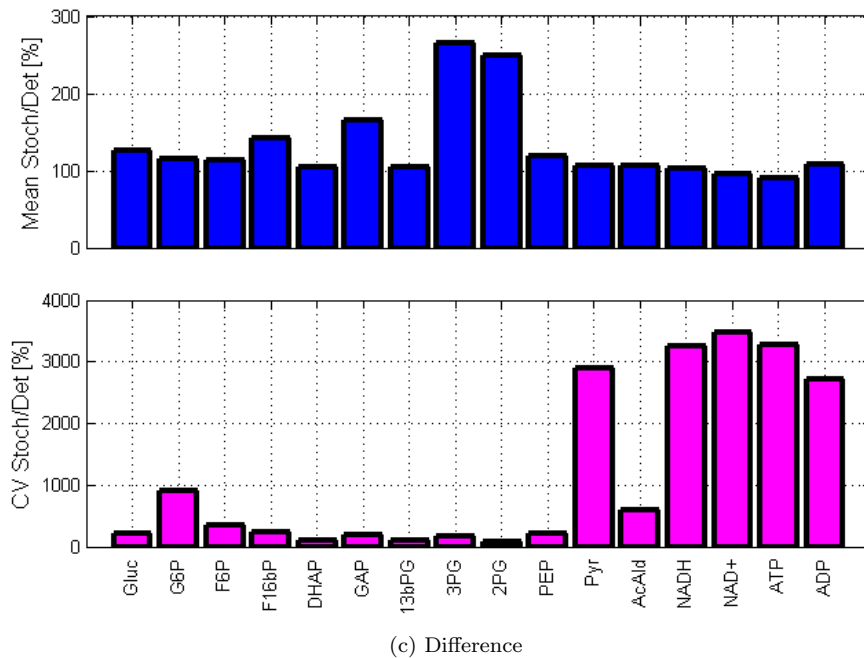
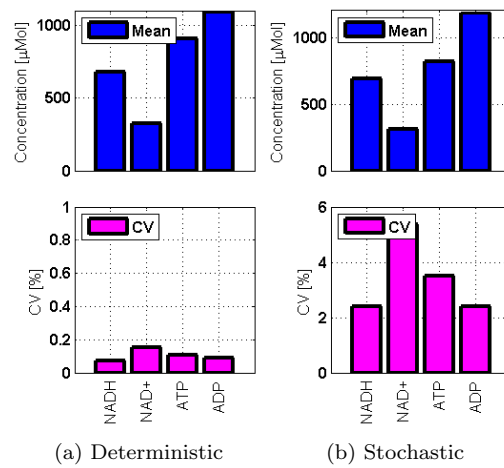


Figure 4.16: Deterministic and stochastic results for the glycolysis system with reversibility and $\lambda = 0.8$, $\mu_C = 0.4$.

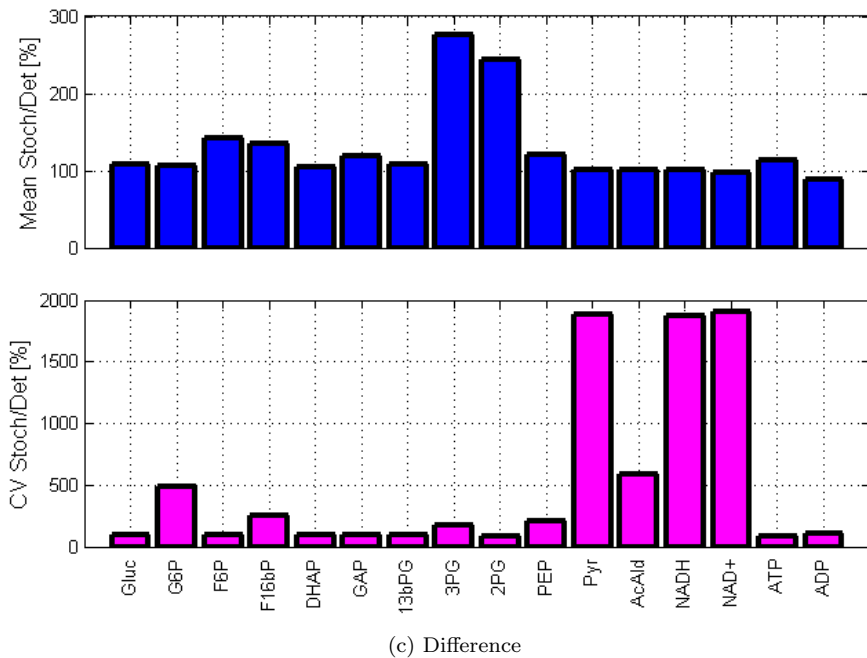
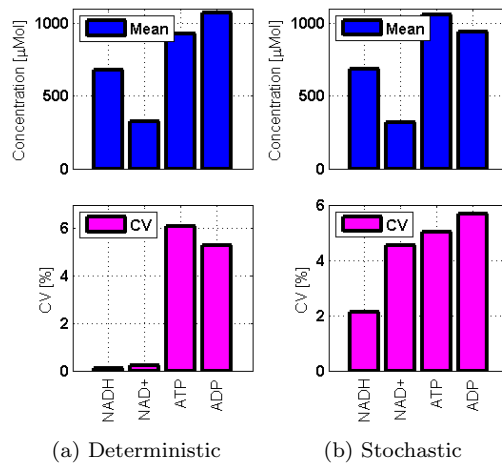


Figure 4.17: Deterministic and stochastic results for the glycolysis system with reversibility, feedback and $\lambda = 0.8$, $\mu_C = 0.4$.

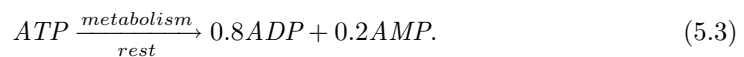
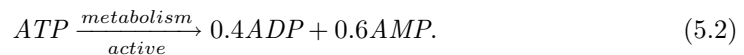
Chapter 5

Adenylate transitions

In Chapter 4 the glycolysis pathway has been modeled as a DEM and a convertor has been added to analyze steady-state behavior. In this chapter the convertor is replaced with energy transitions by energy molecule equilibrating enzyme *ADK* and metabolic reactions, as can be seen by the intersected boxes in Figure 2.1. These energy transitions should function the same as the simple convertor. For convenience the term "adenylate" is slightly abused by restricting its meaning to adenosine 5-mono-, di- and triphosphate—*AMP*, *ADP* and *ATP*, respectively. Adenylate concentrations in a typical cell are: $C_{ATP} = 10 \cdot C_{ADP} = 100 \cdot C_{AMP}$. In the glycolysis pathway the overall adenylate transition is:



meaning that for a steady-state simulation the *ADP* buffer will deplete and the *ATP* buffer will fill up. Metabolism, the set of chemical reactions that occurs in living organisms to maintain life, requires *ATP*. Some metabolic reactions, especially involving resting functions like the Na^+/K^+ pump, reduce *ATP* to *ADP*, and others, especially macromolecular synthesis, degrade *ATP* to *AMP*. Therefore, the relative fractions of these two reactions, $ATP \rightarrow ADP$ and $ATP \rightarrow AMP$, vary depending on how active the cell is, especially how many new macromolecules it is synthesizing. The relation between the products of metabolism, *ADP* and *AMP*, depends on the state of the cell, this can be from resting to active. As a start, the metabolism process is introduced as in an active or in a resting state:



Since conversion from *ATP* to *ADP* or *ATP* to *AMP* are different processes, two drains with different rates are used in the model:

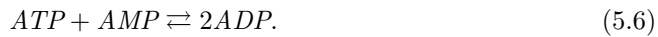


Table 5.1: Adenylate rates.

Process	Rate
Glycolysis	1.00
Metabolism [$ATP \rightarrow ADP$]	1.00
Metabolism [$ATP \rightarrow AMP$]	1.33
ADK	200.00

These rates are linked to each other by $\mu_2 = 1.5\mu_1$ and $\mu_2 = 0.25\mu_1$ to represent an active or a resting cell, respectively. When discussing stability in Section 5.2.4, these relations are used as boundaries for a reasonable metabolism rate.

Another important process concerning the cellular energy homeostasis is enzyme adenylate kinase ADK that catalyzes a reaction between the adenylate molecules. The reaction catalyzed by this enzyme is:



This reaction is sufficiently fast in cells to maintain the reactants at their equilibrium concentrations, and therefore plays an important role in cellular energy stabilization. Another important property of this reaction is that ADK is recognized as a sensitive reporter of the cellular energy state, translating small changes in the balance between ATP and ADP into relatively large changes in AMP concentration. This enables enzymes and metabolic sensors that are affected by AMP to respond with higher sensitivity and fidelity to stress signals [6].

Forward and backward reaction rates are approximately equal in the cellular environment, and always very fast, so:

$$C_{ATP} \cdot C_{AMP} \approx C_{ADP}^2. \quad (5.7)$$

A schematic overview of the adenylate transitions is presented in Figure 5.1. The rates of all processes, normalized to glycolysis are shown in Table 5.1. The reaction rate of ADK is much faster and the energy molecules will therefore be brought into an equilibrium according to 5.7 after each change in concentrations caused by metabolism or glycolysis.

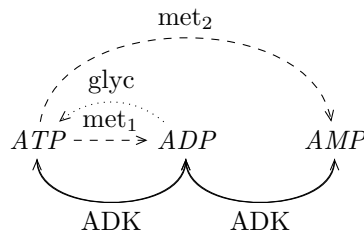


Figure 5.1: Adenylate transitions.

5.1 Energy charge

To have a measure of the content of adenylate molecules, Atkinson introduced the term energy charge [2]. Energy charge φ is used as a dimensionless value for the energy balance in the cell, depending on the relation between adenylate concentrations, see (5.8).

$$\varphi = \frac{[ATP] + 0.5[ADP]}{[AMP] + [ADP] + [ATP]}. \quad (5.8)$$

The energy charge is something that the cell regulates homeostatically. Precisely why is unclear. Energy charge is usually maintained quite close to 1 (typical measures are between 0.95 and 0.98). In our simulations energy charge φ has been tracked, if it goes down (below 0.85) in a stable system we're leaving physiologically reasonable ground. This indicates that either the model is wrong or it's predicting pathology.

The DEM representation of the glycolysis model with the adenylate transitions is presented in Figure 5.2. An abstraction of the glycolysis pathway is presented by the thick box named *Glycolysis*. The *ADP* and *ATP* buffers are not included in this box since they play an important role in the energy balance. The energy charge is calculated in process φ , represented by the dotted circle. This process tracks the concentrations of the adenylate molecules, represented by the dotted lines. From now on, this system will be called the 'energy balance' system.

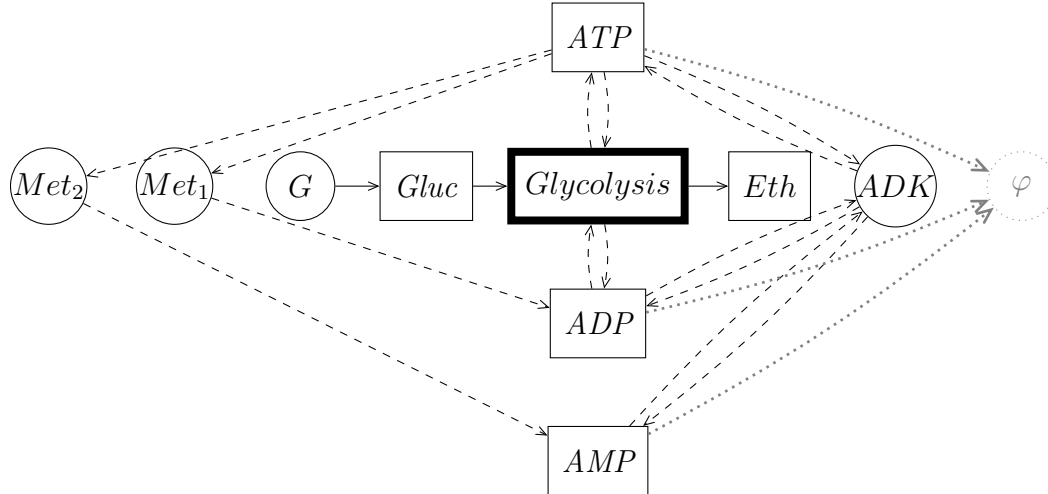


Figure 5.2: DEM representation of the glycolysis pathway with adenylate transitions and energy charge φ .

5.1.0.1 Cell death

If the energy charge drops below a certain level, the cell can't sustain the membrane and the cell dies [3]. In this report it is assumed that if the energy charge drops below 0.70 the cell dies instantaneously. We are focussing on cell death since cells die for no apparent reason and that this might be caused by fluctuations of the energy charge in an otherwise stable system. This hypothesis will be investigated in Chapter 6.

5.2 Stability

Addition of the metabolic reactions and equilibrating enzyme *ADK* to the glycolysis pathway is thought to stabilize the energy balance. More specifically, here the system is assumed to be stable if there is no buildup in the buffers and the mean energy charge is close to unity (about 0.95). If the energy charge drops below 0.70 the system will also be labeled unstable. The system depends on three variables, *Gluc* influx λ , metabolic reaction rate from *ATP* to *ADP* μ_1 and metabolic reaction rate from *ATP* to *ADP* μ_2 . Simulations with the system varying these input variables resulted in some different regions, presented and explained in the following subsections.

5.2.1 Unstable, influx rate too high

There are two cases where the system becomes unstable if the *Gluc* influx rate is too high. First, if the influx exceeds the enzymic capacity. This results in a build up of molecules in the buffer since not all molecules can be handled. Second, if the *ADP* buffer is drained by glycolysis and the metabolic reactions and enzyme *ADK* can't stabilize it, eventually buffer *GAP* blows up, see Figure 5.3. What happens here is that enzyme *PYK* is inhibited by the lack of *ADP*. Enzymes downstream of the pathway work with the same rate as *PYK*, which results in depletion of *NAD*⁺. This depletion slows down enzyme *GAPDH*, resulting in *GAP* buildup.

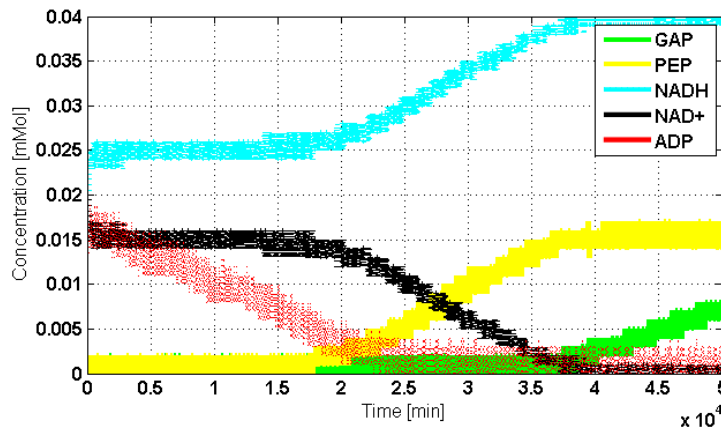


Figure 5.3: Buffer contents of *GAP*, *PEP*, *ADP*, *NADH* and *NAD*⁺.

5.2.2 Unstable, metabolic ATP demand too high

When the metabolic reactions require a lot of *ATP* molecules and both glycolysis and enzyme *ADK* are insufficient to keep the *ATP* concentration at a constant level, the system becomes unstable. The *Gluc* buffer eventually blows up since *ATP* is required for the first reaction. Simulation results of the unstable system due to a exceeding metabolic demand are presented in Figure 5.4. This figure shows the adenylate concentrations in the upper figure, energy charge in the middle figure and the amount of molecules in the system, labeled as work in progress (WIP). It can be seen that the *ATP* concentration constantly decreases, resulting in an increase in *AMP* and decrease of the energy charge.

When the *ATP* buffer has been depleted, the system can't reconfigure any incoming molecules and the WIP increases.

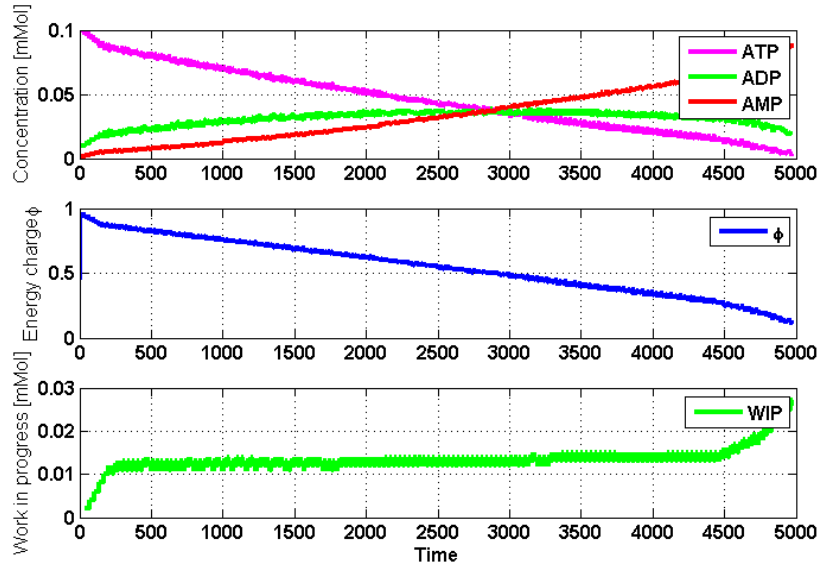


Figure 5.4: Unstable system, metabolic reactions too fast, $\lambda = 0.02$, $\mu_1 = 0.03$ and $\mu_2 = 0.03$.

5.2.3 Unstable, insufficient metabolic ATP demand

If the metabolic *ATP* demand is insufficient to handle the *ATP* increase by glycolysis, the system blows up in the *AcAld* buffer, as presented in Figure 5.3. Simulation results are presented in Figure 5.5. The energy charge stays very close to 1, since the *ADP* and *AMP* concentrations are almost zero. Enzyme *ADK* can't stabilize this system either, since *AMP* is required to diminish the *ATP* concentration.

5.2.4 Stable

For a small region of input variables the deterministic system is stable, simulation results of a stable system are presented in Figure 5.6. It can be seen that after an initial phase, the adenylate concentrations, energy charge and WIP remain at a constant level. For the metabolic reaction rates to be physiologically reasonable, these rates must be somewhere between an active and resting cell, as expressed in (5.2) and (5.3). The relation between μ_1 and μ_2 is shown in (5.9), and this area is presented in Figure 5.7. The upper edge represents an active cell and the lower edge represents a resting cell.

$$0.25\mu_1 \leq \mu_2 \leq 1.5\mu_1 \quad (5.9)$$

In order to find the stability region the adenylate concentrations must be investigated. The rates in which the adenylate concentrations change depends on input rate λ and

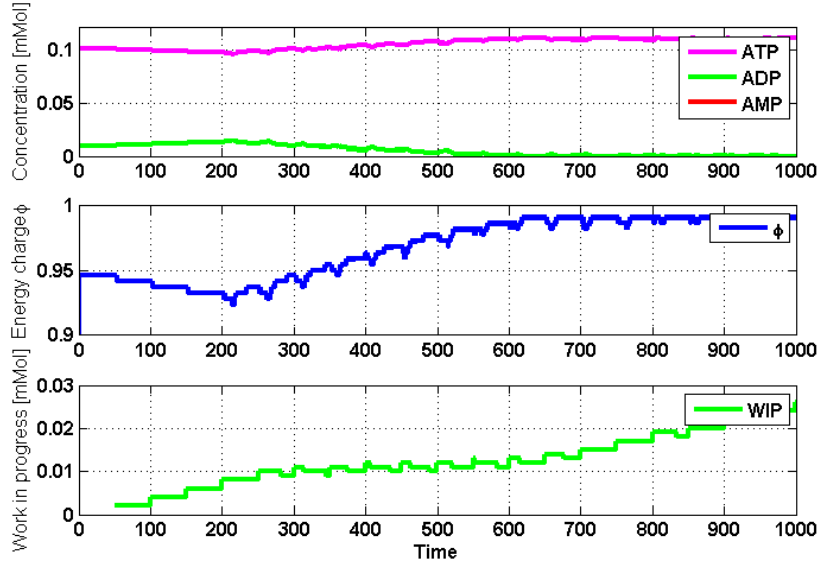


Figure 5.5: Unstable system, metabolic reactions too slow, $\lambda = 0.02$, $\mu_1 = 0.00$ and $\mu_2 = 0.00$.

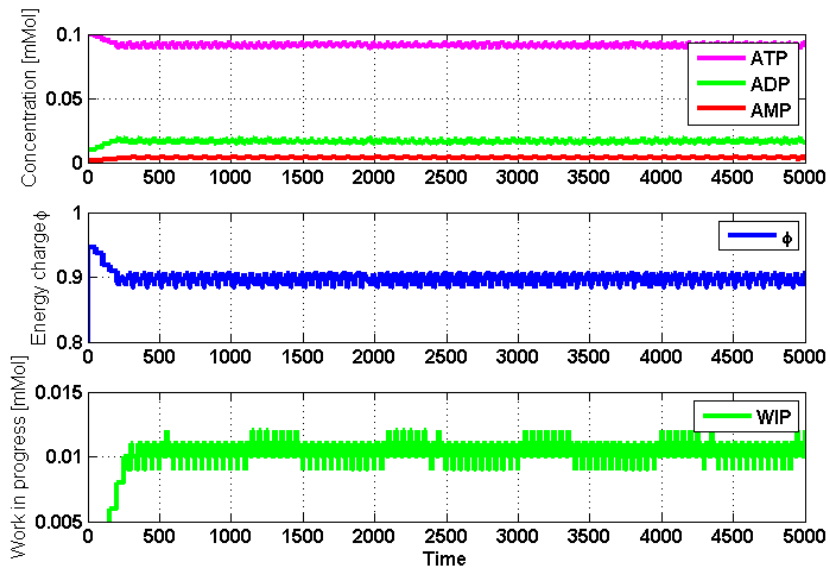


Figure 5.6: Stable system, $\lambda = 0.02$, $\mu_1 = 0.02$ and $\mu_2 = 0.01$.

metabolic reaction rates μ_1 and μ_2 :

$$r_{ATP} = 2\lambda - \mu_1 - \mu_2, \quad (5.10a)$$

$$r_{ADP} = -2\lambda + \mu_1, \quad (5.10b)$$

$$r_{AMP} = \mu_2, \quad (5.10c)$$

where r_x denotes the rate of concentration change of molecule x . Enzyme *ADK* keeps the adenylate concentrations in equilibrium, see (5.7). *ADK* stabilizes the system if the sum

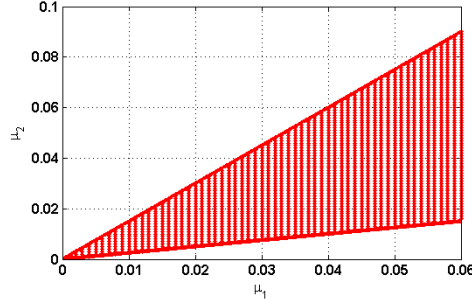


Figure 5.7: Area of reasonable metabolic input rates.

of the rates of *ATP* and *AMP* are opposite to the rate of *ADP*. Also the rates of *ATP* and *AMP* must be similar to prevent a build-up in the system:

$$r_{ATP} + r_{AMP} = -r_{ADP}, \quad (5.11a)$$

$$r_{ATP} = r_{AMP}. \quad (5.11b)$$

Combining (5.10) and (5.11) shows that the system can be stable if the input variables satisfy (5.12).

$$2\lambda - \mu_1 - 2\mu_2 = 0. \quad (5.12)$$

In all cases enzyme *ADK* reconfigures *ATP* and *AMP* into *ADP*. The backward *ADK* reaction is not possible since it requires an diminishing *AMP* concentration, what is not possible in the current setup.

Another restriction on the stability of the system is the maximal rate in which the incoming molecules can be handled. The system is assumed to be stable if all incoming molecules can be handled, e.g. no accumulating buffer levels, and if the mean energy charge level stays above 0.85. Mean energy charge decreases with increasing λ , see Figure 5.8. If λ exceeds 0.055, the overall energy charge drops below 0.85 and the system is unstable. Mean φ for the stable system is about 0.89, and is close to 0.95 in actual cells. The total set of input values that result in a stable system is presented in Figure 5.9. The red section represent the values that are in the reasonable metabolic area. It can be seen that this is a very specific region.

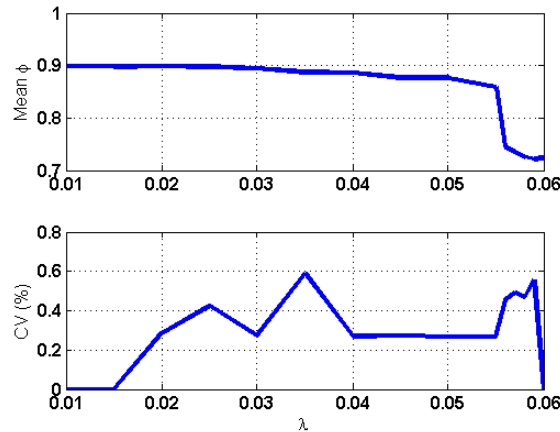


Figure 5.8: Mean energy charge and CV versus input rate λ .

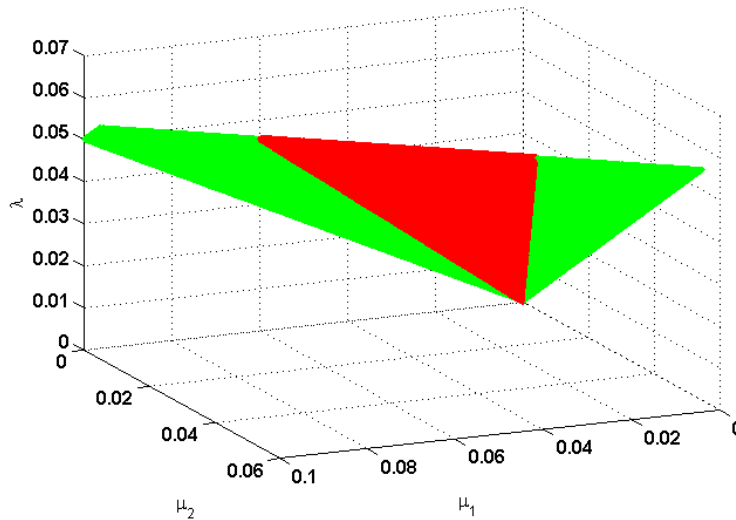


Figure 5.9: Input parameter combinations resulting in a stable deterministic system.

5.2.5 Unstable, stochastic influence

It is clear that the energy balance system can be stable with deterministic values. If stochastic distributions are used the system becomes unstable, independent of the input variables. Simulation results of the system with stochastic distributions are presented in Figure 5.10. Similar input variable values as in Figure 5.7 have been used. The stable system becomes unstable when stochastic distributions are used instead of deterministic values. The time it takes for the energy charge in simulations with the stochastic system to drop below 0.70 is presented in Figure 5.11. This figure contains results of 10000 simulations and shows that in 95% of the simulations, the system becomes unstable within $2 \cdot 10^4$ time units. Looking at cell environment, nothing is exactly deterministic and this would result in an unstable energy balance when only the glycolysis pathway, metabolic reactions and enzyme *ADK* are considered. In Chapter 6 downstream regulation has been implemented to stabilize this system.

5.3 Conclusion

The glycolysis pathway has been extended with metabolic reactions, reconfiguring *ATP* into *ADP* and *AMP* and adenylate equilibrating enzyme *ADK* in order to stabilize the energy molecule concentrations. It has been showed that this deterministic system got a very small region of input variable values resulting in a stable system. If stochastic distributions are used the system always results unstable, independent of the input variables.

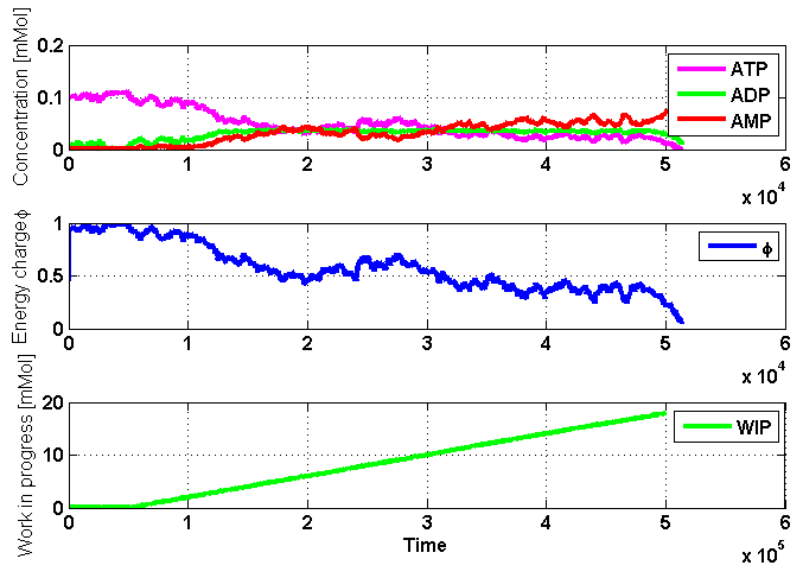


Figure 5.10: Unstable stochastic system, $\lambda = 0.02$, $\mu_1 = 0.02$ and $\mu_2 = 0.01$.

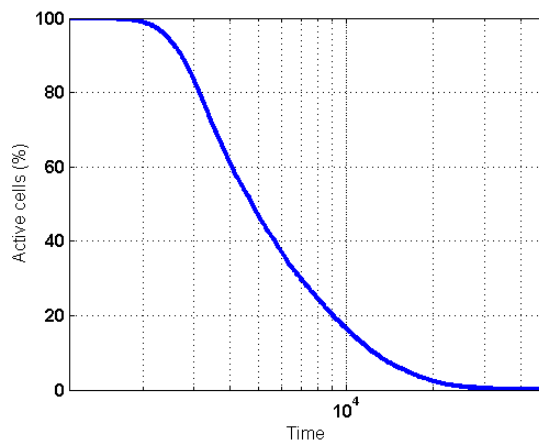


Figure 5.11: Time it takes for the stochastic system to become unstable.

Chapter 6

Energy balance regulation

The energy balance system consisting of the glycolysis pathway, metabolic reactions and enzyme *ADK* can not be stabilized by the input variables when using stochastic distributions. A stable system could be obtained by adding more reactions as shown in [11], or by regulating the *Gluc* influx. This chapter presents the latter approach in several ways.

In order to maintain the energy charge near the desired level, the cell regulates the *Gluc* influx by putting more or less glucose receptors on the membrane. The receptors have got a certain death rate, therefore the influx of *Gluc* can be decreased or increased depending on the rate glucose receptors are placed. In this chapter, two feedback regulators have been implemented in the model. The robustness of the regulator, stochastic influences and adding a time delay have been investigated. Section 6.1 presents a regulator feedback based on the energy charge and Section 6.3 presents feedback based on the *ATP/AMP* ratio. In Section 6.4, regulation according to (5.12) is presented and the first steps towards a continuous regulator are taken in Section 6.5.

6.1 Regulation by energy charge

In order to keep the energy charge at a constant level, the cell asks for more *Gluc* molecules when energy charge ϕ is low. When more *Gluc* molecules enter the glycolysis pathway, more *ADP* molecules are reconfigured into *ATP* molecules and the energy charge increases. However, in the first steps of the glycolysis pathway *ATP* is reconfigured into *ADP* and this means an extra drop in the energy charge before it increases. If ϕ exceeds a certain level the *Gluc* influx is decreased, resulting in a lower energy charge due to a lower *ATP* production. It is not exactly clear how the energy charge is measured in the cell and how this leads to a change in influx. To examine if a regulation based on ϕ stabilizes the system, the energy charge is calculated in a separate process, see Figure 6.1. The red dotted lines represent data going to process ϕ that calculates the energy charge. ϕ is connected to *Gluc* influx λ by the blue dotted channel.

As a start, the regulation scheme used is a three-way switch depending on the energy

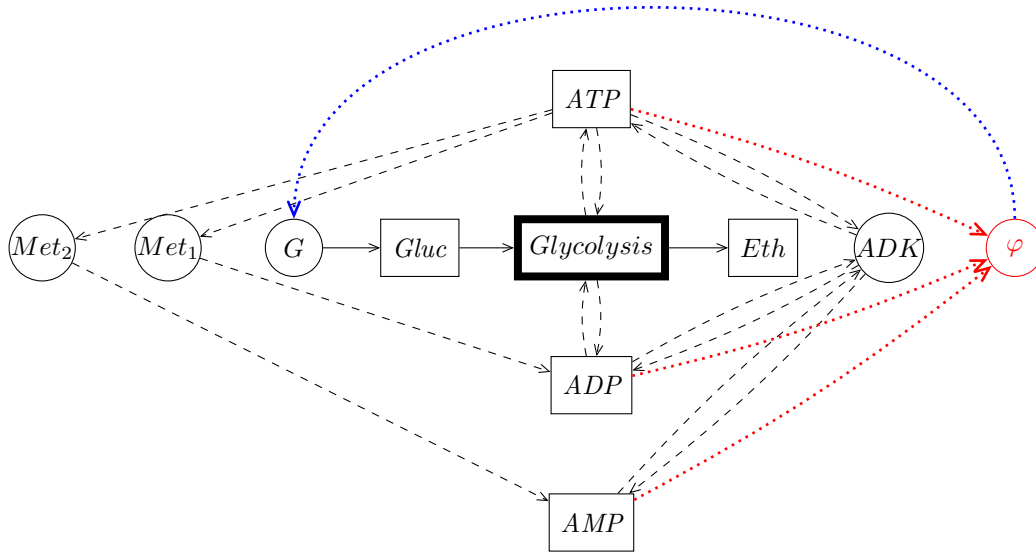


Figure 6.1: DEM representation with regulation based on φ

charge, presented in (6.2) with λ_0 the initial influx rate. A graphical representation of this regulator is presented in Figure 6.2.

$$\lambda = \begin{cases} 1.5 \cdot \lambda_0 & \text{if } \varphi < 0.90 \\ \lambda_0 & \text{if } 0.90 \leq \varphi \leq 0.98 \\ 0.25 \cdot \lambda_0 & \text{if } \varphi > 0.98 \end{cases} \quad (6.1)$$

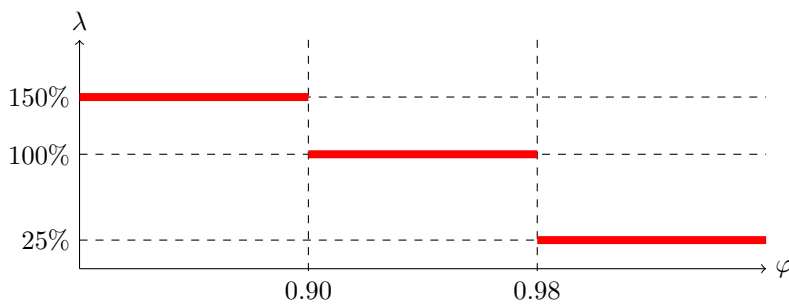


Figure 6.2: *Gluc* influx rate λ depending on the energy charge level.

This link results in a stable system for input variables outside the stable area presented in Section 5.2.4, see Figure 6.3. Simulations results of a deterministic system with $\lambda = 0.025$, $\mu_1 = 0.015$, $\mu_2 = 0.017$ are presented, which is a little outside the stable region presented in Figure 5.9. Average energy charge is 0.96. The lower figure shows the influx over time, it can be seen that the influx rate has been decreased for a short period with periodic intervals, lowering the energy charge. Due to stochastic distributions in the system, the energy charge fluctuates much more, see Figure 6.4. φ even reaches a value of 0.61 what in the cell means instant death. However, φ of the stochastic system will not go down to 0.60 or lower in contrast to the system without regulation. So essentially the feedback

regulator stabilizes the system but due to the energy charge constraint of 0.70 the system will be labeled unstable. These simulations also show that even if a deterministic system is very stable, stochastic distributions in the system can cause a dramatic decrease of the energy charge.

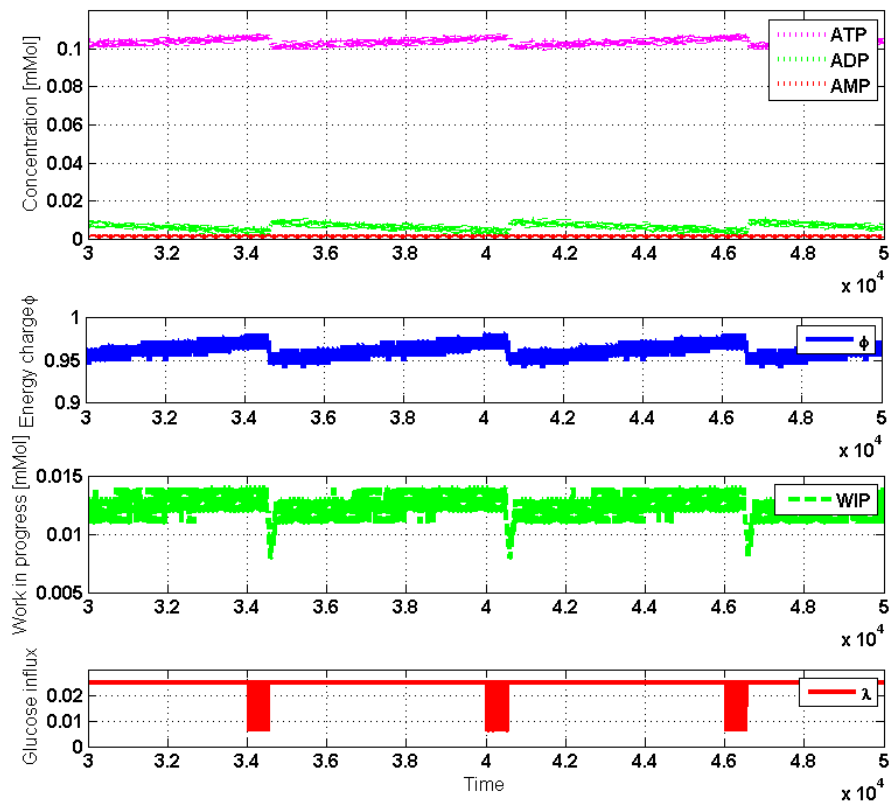


Figure 6.3: Deterministic simulation results with $\lambda = 0.025$, $\mu_1 = 0.015$, $\mu_2 = 0.017$.

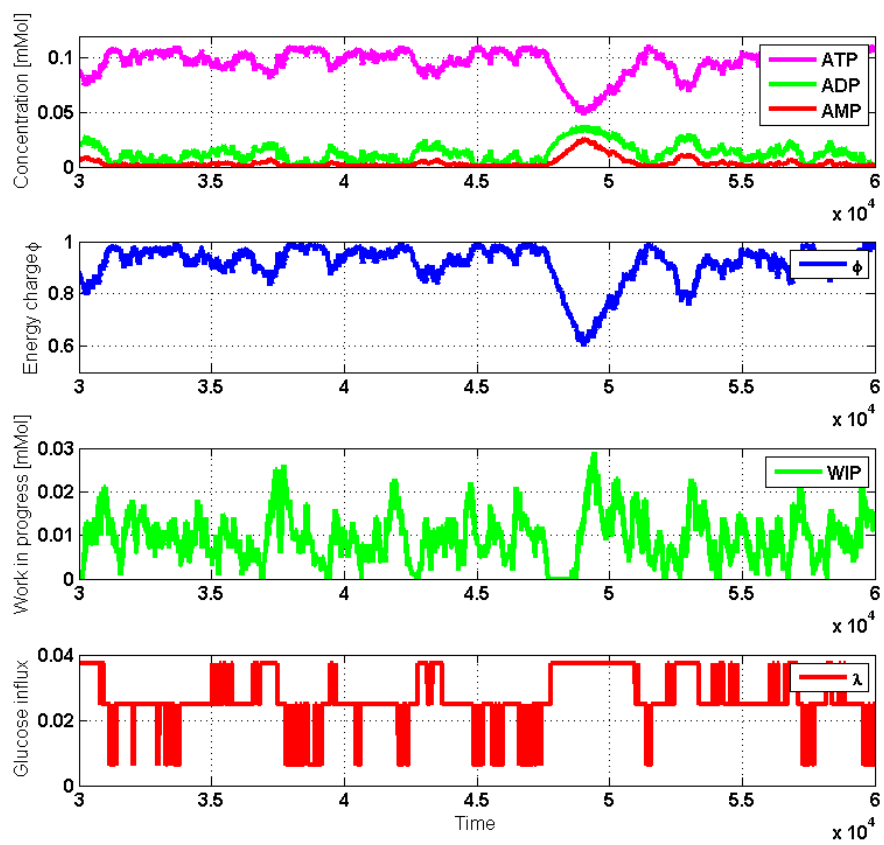


Figure 6.4: Stochastic simulation results with $\lambda = 0.025$, $\mu_1 = 0.015$, $\mu_2 = 0.017$.

6.1.1 Robustness

The robustness of the regulator, i.e. the ability of keeping a stable system, has been investigated by varying the *Gluc* influx rate λ , and metabolism rates M_1 and M_2 (conversion of *ATP* to respectively *ADP* and *AMP*). The deterministic system has been used, and the system is assumed to be stable if there is no build-up in the buffers and the mean energy charge is higher than 0.85. The red dots represent the set of parameters that are reasonable values for the metabolic reactions. It can be seen that the system with regulation is stable for a much bigger area than the system without regulation, as expected.

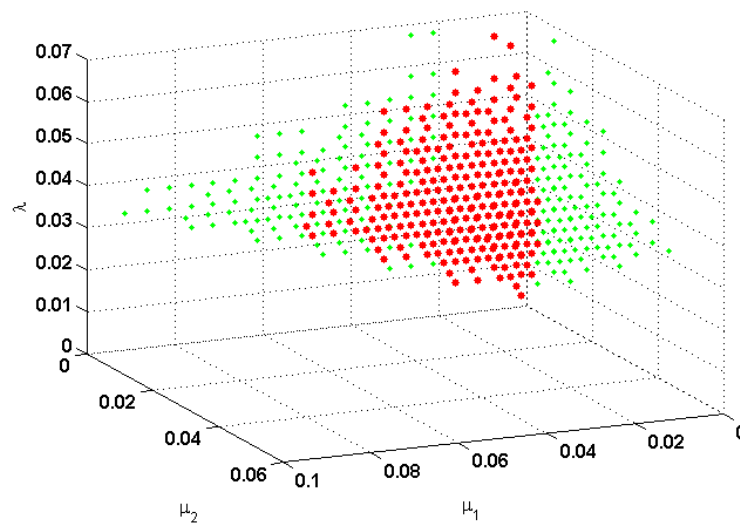


Figure 6.5: Robustness regulator, time = 1.000.000.

Figure 6.6 shows the difference between simulations of the stochastic system with parameters in the deterministic stable region ($\lambda = 0.025, \mu_1 = 0.02$ and $\mu_2 = 0.015$), represented by the blue line, and stochastic simulations with parameters outside the deterministic stable region ($\lambda = 0.025, \mu_1 = 0.03$ and $\mu_2 = 0.02$), represented by the red line. Each line shows the time it takes for the energy charge to reach 0.7 over 1000 simulations. It can be seen that the difference between cell death of the system with parameters on the deterministic stable region and the system with parameters on the edge of the deterministic regulated system differ a lot. Mean time for cell death is 45 times longer for the system with parameters on the deterministic stable region. Mean energy charge of the regulated system, with varying influx rate, is presented in Figure 6.7. With increasing influx rate, average energy charge increases. The average energy charge of the stable system is 0.94, what is very close to the desired level.

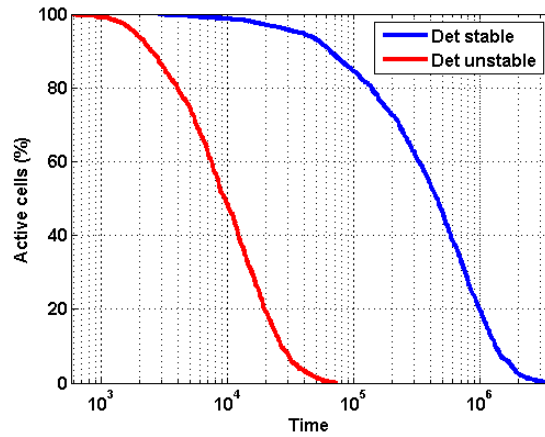


Figure 6.6: Death rate of the cell for a system with parameters inside the stable region and on the edge of the regulated stable region.

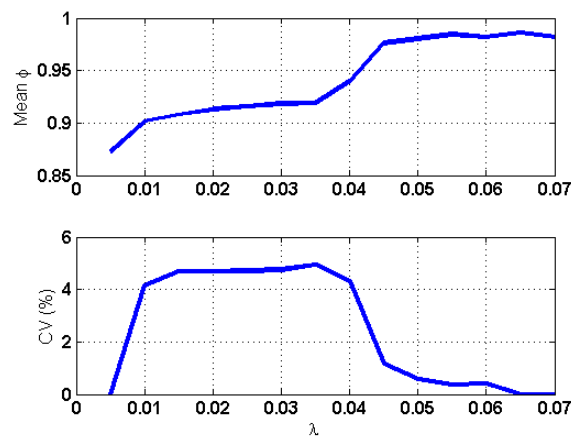


Figure 6.7: Mean energy charge and CV versus input rate λ .

6.1.2 Time delay

Feedback from energy charge φ to *Gluc* influx λ in the DEM occurs instantaneously. In the cell, there is a delay between reaching a threshold value and the actual change of *Gluc* influx since it takes some time for the glucose receptors to reach the membrane. Therefore, a time delay denoted by δ has been introduced in the model. This delay has been modeled between the time φ reaches a threshold value and an actual change in influx. This time delay does result in a significant difference for the deterministic system. Figure 6.8 shows the influence of feedback on the death rate of the cell for the stochastic system. It is assumed that the cell dies when $\varphi \leq 0.7$. The blue line shows the system with feedback without a time delay in the feedback. Feedback with a time delay of 100 is presented by the red line. Results of feedback with a time delay of 1000 time units is presented by the magenta line. It can be seen that implementing a time delay in the feedback results in a faster death rate, as expected. Cell death of the system without feedback is represented by the green line. The distributions of the system with feedback and system without feedback are also different.

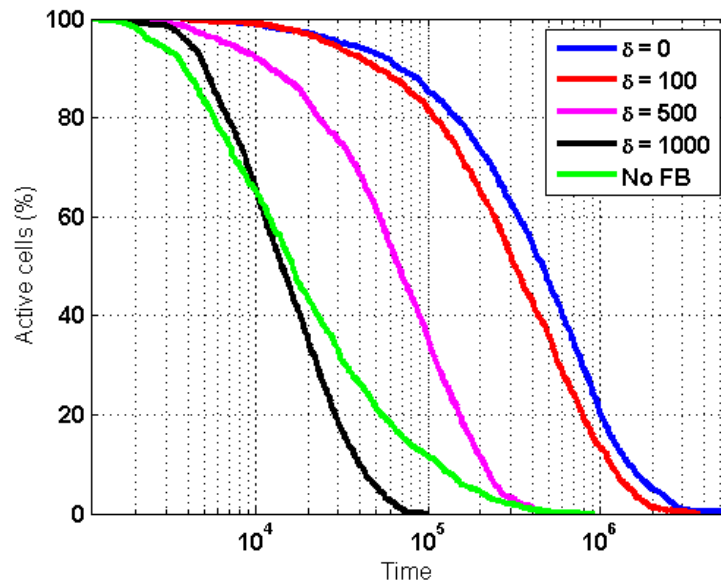


Figure 6.8: Death rate of the cell with and without feedback based on the energy charge.

Results of tracking the number of times the energy charge reaches a certain threshold and the percentage of total time under these thresholds are presented in Table 6.1. The simulation time is $1 \cdot 10^6$ time units. Two cases are presented, one with parameters inside the deterministic stable region and the other outside this region. In the latter case the energy charge reaches the thresholds more and spends more time under these thresholds. In both cases, implementing a time delay has a negative effect on the energy charge and in all cases the energy charge never stays above 0.60. Figure 6.9 gives a graphical representation of the time spent under the thresholds, depending on the time delay.

Table 6.1: Simulation results of energy charge regulation.

δ	< 0.9	< 0.9	< 0.8	< 0.8	< 0.7	< 0.7	< 0.6
[time]	[%]	[number]	[%]	[number]	[%]	[number]	[%]
$\lambda = 0.025, \mu_1 = 0.015, \mu_2 = 0.017$							
0	22.23	302867	0.84	18233	0.04	832	-
100	24.11	298289	1.23	23877	0.10	1762	-
500	33.66	226253	4.71	67843	0.31	6793	-
1000	41.83	139150	15.39	104147	2.62	39674	-
$\lambda = 0.024, \mu_1 = 0.015, \mu_2 = 0.017$							
0	26.33	325714	1.15	23607	0.09	1413	-
100	28.14	316322	1.51	30663	0.10	1789	-
500	36.83	237070	5.48	75375	0.43	8046	-
1000	44.68	147243	16.85	107300	3.16	44083	-

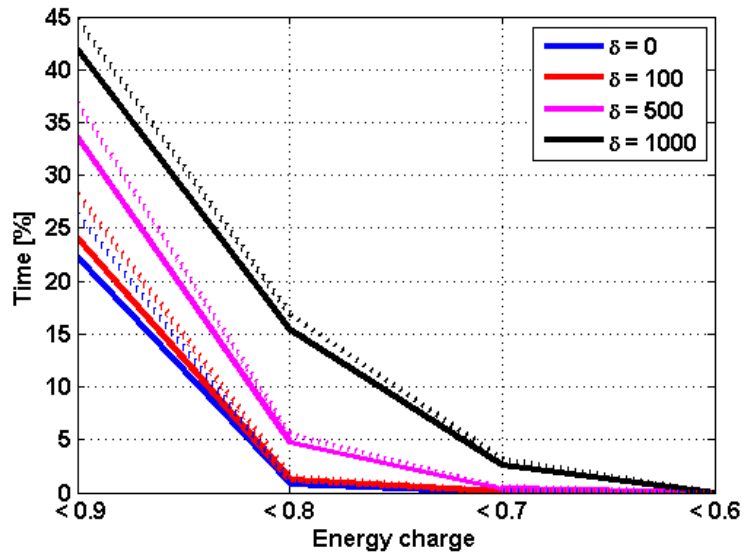


Figure 6.9: Time spent under a certain energy charge level, $\lambda = 0.024$ is represented by the dotted lines and $\lambda = 0.025$ by the solid lines.

6.2 Molecule concentration analysis

The mean buffer levels and fluctuations in these levels of the energy balance system regulated with the energy-charge dependent regulator, are presented in this section. The approach is similar as in Section 4.5 and simulations have been performed with different input parameters. Initial concentrations for the simulations are:

$$\begin{aligned}C_{ATP}(0) &= 100\mu\text{Mol} \\C_{ADP}(0) &= 10\mu\text{Mol} \\C_{NADH}(0) &= 10\mu\text{Mol} \\C_{NAD^+}(0) &= 10\mu\text{Mol} \\\lambda, \mu_1 \text{ and } \mu_2 &\text{ vary.}\end{aligned}$$

Simulation results of the system with input parameters inside the feasible deterministic stable region from Figure 5.9 are presented in Figure 6.10. The input parameters are: $\lambda = 0.02$, $\mu_1 = 0.02$ and $\mu_2 = 0.01$. Figure 6.10a shows the mean value of the energy molecules concentration and the coefficient of variation (CV) of these buffer levels for simulations with the deterministic system. Figure 4.16b presents the mean and CV for simulations with stochastic distributions and Figure 6.10c shows the difference between the deterministic and stochastic results for all buffer levels.

It can be seen that the CV of *ATP* is low compared to the other energy molecules, this can be explained by the fact that there are a lot more *ATP* molecules present in the system and a similar fluctuation in all energy molecules would result in a lower CV for *ATP*. Furthermore, the comparison between results of simulations with the deterministic and stochastic system show a big increase in CV for the energy molecule buffer levels, similar to the results of the glycolysis pathway shown in Section 4.5.

Figure 6.11 presents simulation results of the system with input parameters outside the deterministic stable region; $\lambda = 0.025$, $\mu_1 = 0.015$ and $\mu_2 = 0.017$. It can be seen that the difference between stochastic and deterministic results are not that big as for the system with parameters inside the stable region. Furthermore, the difference between the system outside and inside the stable region is that the CV for the energy charge molecule levels is twice as high in the deterministic case.

Another comparison has been performed in order to determine whether the variance in the buffer levels depends on the dynamic state of the system. The results of simulations with a system with active metabolism and a system which represents a resting cell have been compared and these results show no significant difference. Therefore, it is not possible to determine the dynamic state of the system by looking at the mean buffer levels and fluctuations in these levels.

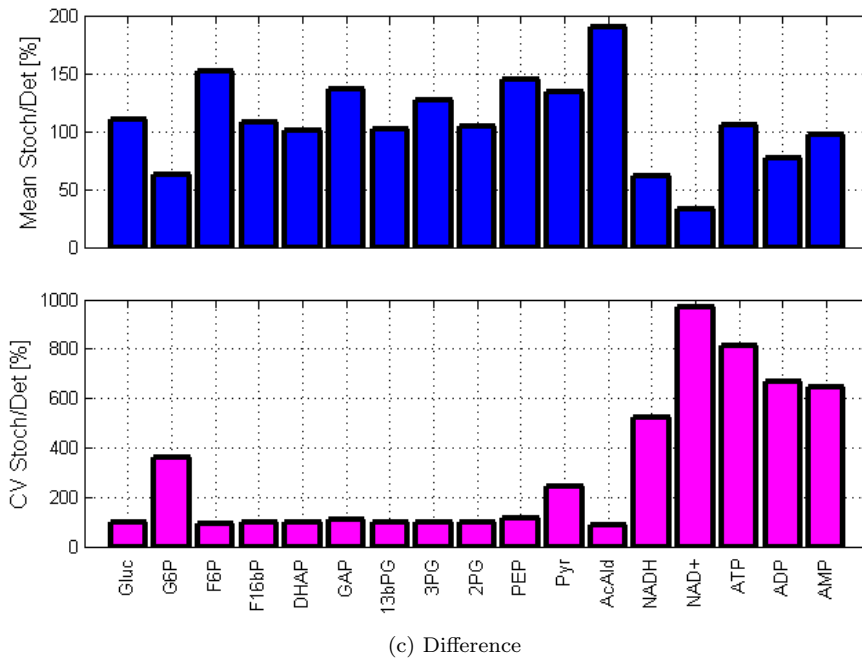
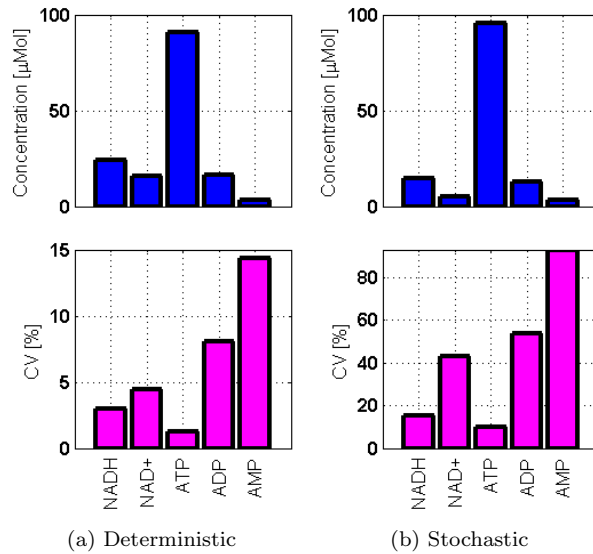
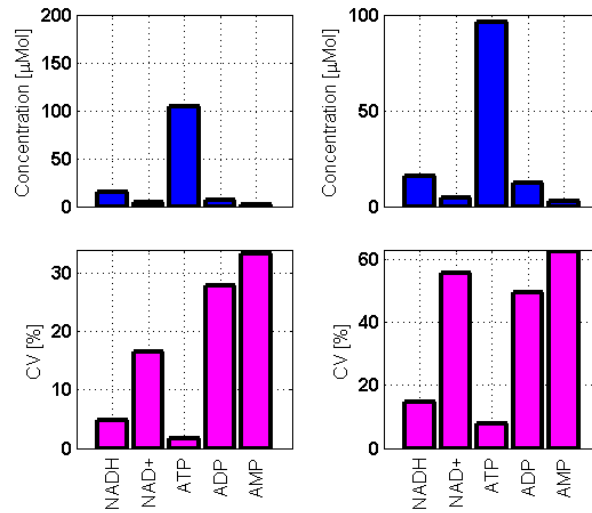
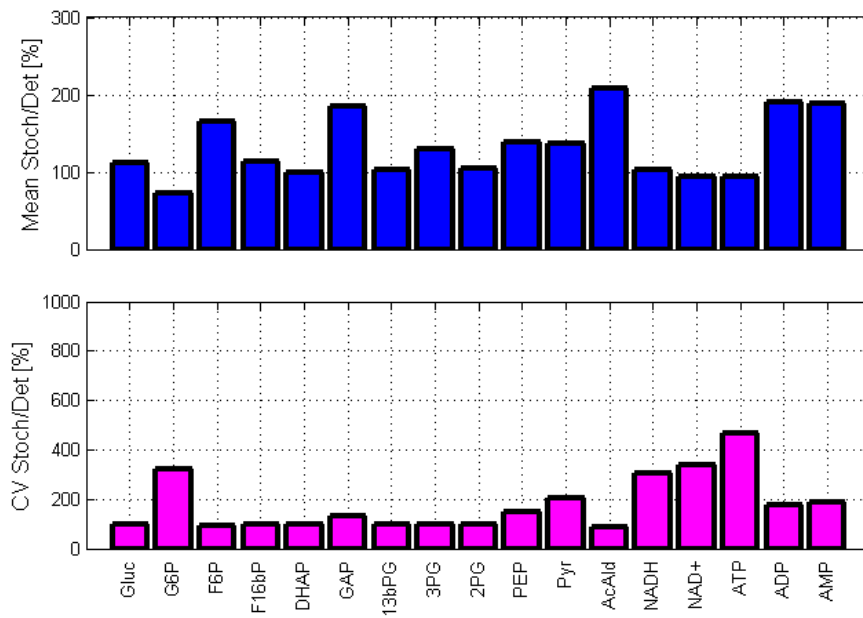


Figure 6.10: Deterministic and stochastic results for a system inside the deterministic stable region; $\lambda = 0.02$, $\mu_1 = 0.02$ and $\mu_2 = 0.01$.



(a) Deterministic

(b) Stochastic



(c) Difference

Figure 6.11: Deterministic and stochastic results for a system outside the deterministic stable region; $\lambda = 0.025$, $\mu_1 = 0.015$ and $\mu_2 = 0.017$.

6.3 Regulation by AMPK

Regulation of the system can be done by tracking the energy charge and depending on the energy charge level altering the glucose influx, as shown in Section 6.1, however it is not clear how the energy charge level is measured in the cell and what causes the glycolysis rate to change. Another regulation approach has been argued in [7]. It is argued that the *AMP*-activated protein kinase *AMPK* works as a kind of "Master-switch" between anabolism (metabolic reactions) and catabolism (glycolysis), since all living cells must maintain a high ratio between *ATP* and *ADP*. Enzyme *AMPK* is activated by a decreasing *ATP* concentration in combination with an increasing *AMP* concentration. It is also argued that, in mammalian cells, *AMPK* is involved in upregulating the *Gluc* uptake. This enzyme acts similar as monitoring the energy charge and giving feedback to the *Gluc* influx, except it does not depend on the *ADP* concentration, but on the cellular *ATP/AMP* ratio denoted by ϑ . The regulation scheme for regulation by *AMPK* is as follows:

$$\lambda = \begin{cases} 1.5 \cdot \lambda_0 & \text{if } \vartheta < 90 \\ \lambda_0 & \text{if } 90 \leq \vartheta \leq 105 \\ 0.25 \cdot \lambda_0 & \text{if } \vartheta > 105 \end{cases} \quad (6.2)$$

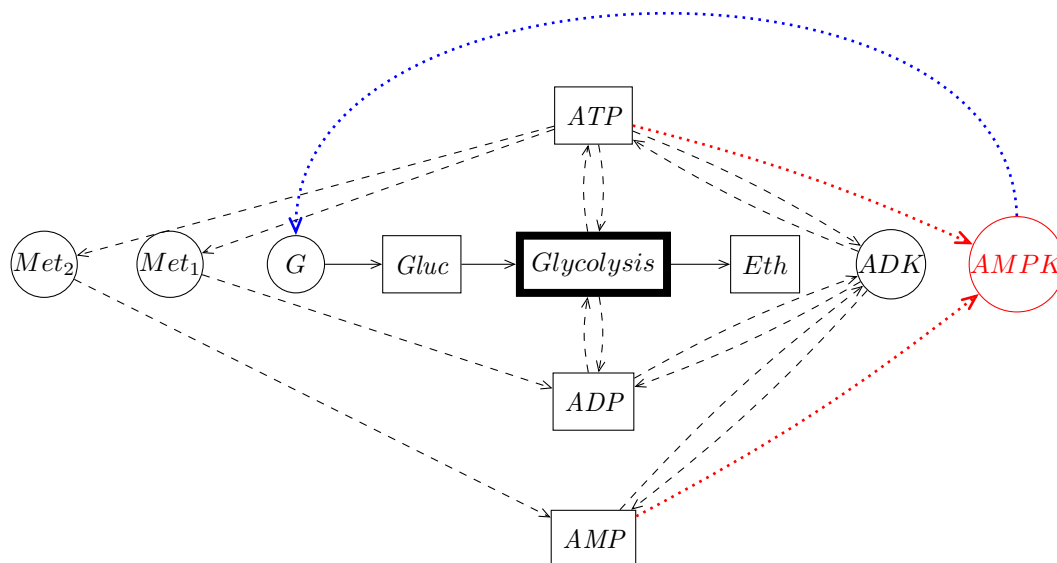


Figure 6.12: DEM representation of the system with *AMPK* regulation

The DEM representation of the system with *AMPK* regulation is presented in Figure 6.12, with the red lines representing the regulator and the blue dotted line represents the feedback. Figure 6.13 shows results of a simulation with the deterministic system regulated by the *ATP/AMP* ratio. Energy charge φ has also been tracked to compare this regulated system with the energy charge regulated system. It can be seen that the system is stable and the mean value of the energy charge is 0.95. The brief drops in ϑ , and corresponding increase in influx rate, occur when metabolism reconfigures an *ATP* molecule into an *AMP* molecule and enzyme *ADK* quickly restores the energy balance. There is a lot of

fluctuation in the ATP/AMP ratio and corresponding change in influx rates since there are few AMP molecules present and a change in this concentration has a big impact on the ratio. Results of the system with stochastic distributions are presented in Figure 6.14. Similar to the energy charge regulated system, a lot more fluctuations occur.

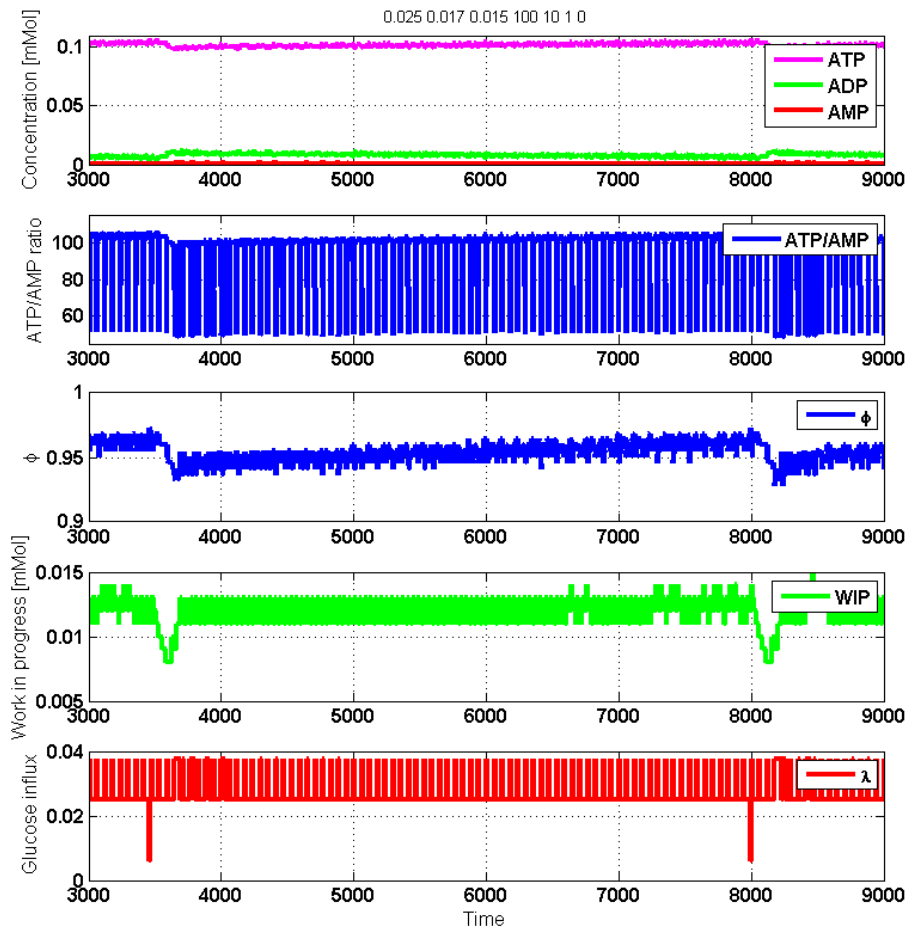


Figure 6.13: Results of simulations with ATP/ADP ratio regulated deterministic system.

6.3.1 Robustness

The robustness of the regulator has been investigated by varying the $Gluc$ influx rate λ , and metabolism rates M_1 and M_2 . The region of input variable values that result in a stable system is presented in Figure 6.15. Compared to the energy charge regulated system in Figure 6.5, the regions of parameters which result in a stable system are almost similar.

Mean energy charge of the $AMPK$ regulated system, with varying influx rate, is presented in Figure 6.16. The average energy charge of the stable system is 0.95, what is exactly

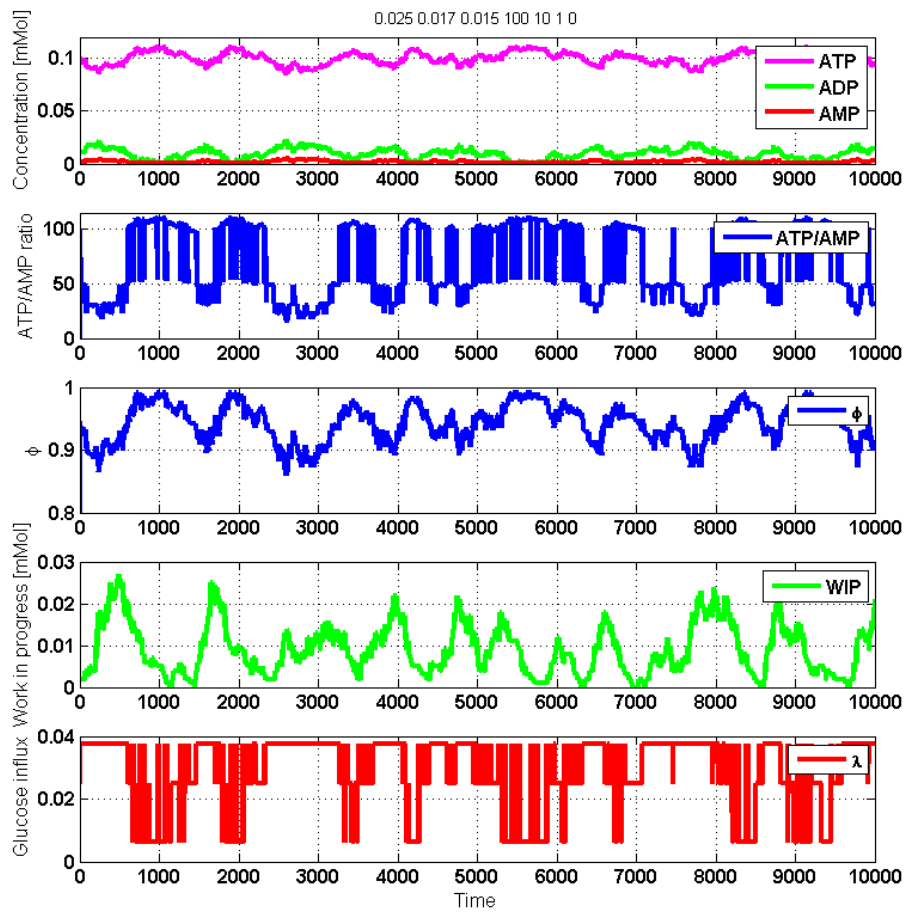


Figure 6.14: Results of simulations with ATP/ADP ratio regulated stochastic system.

the desired level.

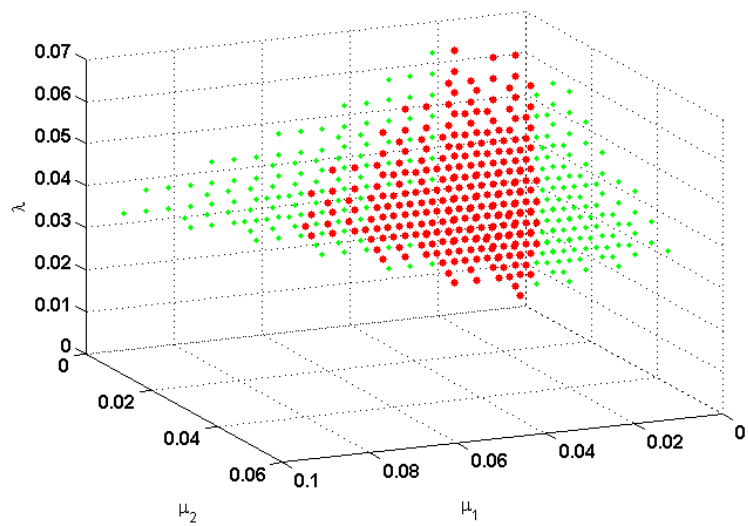


Figure 6.15: Robustness regulator, time = 1.000.000.

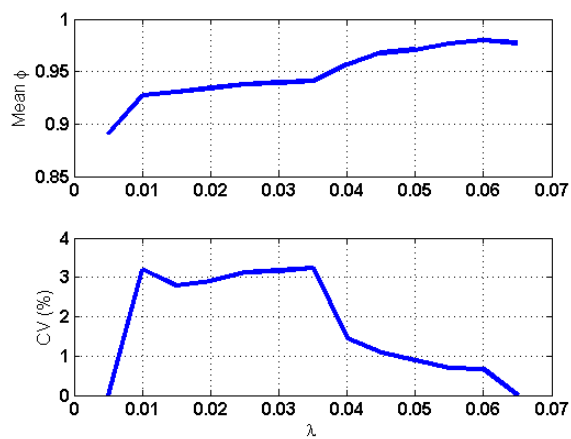


Figure 6.16: Mean energy charge and CV versus input rate λ .

6.3.2 Time delay

In the cellular environment it takes time between reaching a feedback threshold value and actual change in influx rate, as explained in Section 6.1.2. To compare the ATP/ADP ratio regulated system with the system regulated by the energy charge, similar time delays have been used, and the energy charge has been tracked. Figure 6.17 shows the time it takes before the energy charge reaches 0.7 for the system feedback based on the ATP/AMP ratio in solid lines and the system with feedback based on the energy charge in dotted lines. It can be seen that on average the feedback improves the time it takes for the energy charge to reach 0.7, but not as much as the feedback based on the energy charge.

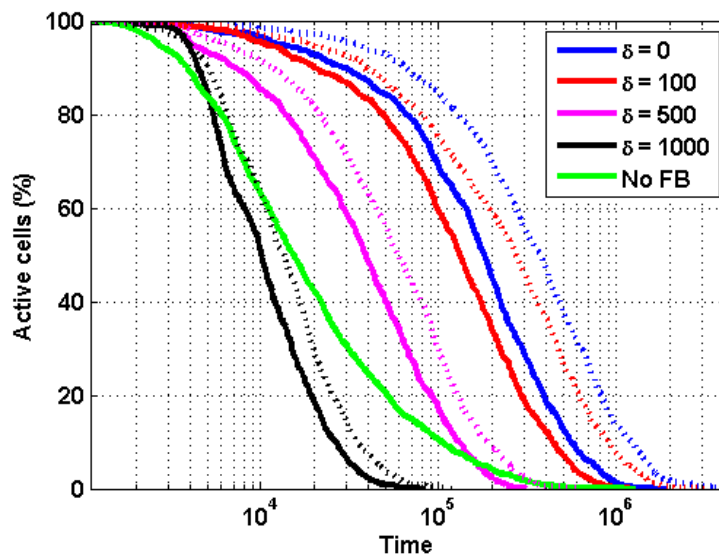


Figure 6.17: Death rate of the cell with and without feedback based on the ATP/AMP ratio (solid lines) compared to feedback based on the energy charge (dotted lines).

Table 6.2 and Figure 6.18 present results of simulations with counting the number and time spent under certain thresholds, as is done with the energy charge regulated system. Compared to these results in Table 6.1, it can be seen that the drops in energy charge below 0.90 are less frequent but more serious as the number of times φ drops below 0.70 is much more.

Table 6.2: Simulation results of *AMPK* regulation.

δ	< 0.9	< 0.9	< 0.8	< 0.8	< 0.7	< 0.7	< 0.6
[<i>time</i>]	[%]	[<i>number</i>]	[%]	[<i>number</i>]	[%]	[<i>number</i>]	[%]
$\lambda = 0.025, \mu_1 = 0.015, \mu_2 = 0.017$							
0	18.34	280397	1.39	21836	0.11	2061	-
100	21.24	273555	1.81	27408	0.16	2802	-
500	34.25	195622	6.03	77265	0.56	10205	-
1000	42.63	122057	17.77	104843	3.51	48480	-
$\lambda = 0.024, \mu_1 = 0.015, \mu_2 = 0.017$							
0	20.85	293921	1.76	26458	0.14	2565	-
100	23.84	285821	2.26	32390	0.23	3757	-
500	36.99	200922	7.08	84400	0.74	12350	-
1000	45.72	124653	19.76	111558	4.28	54044	-

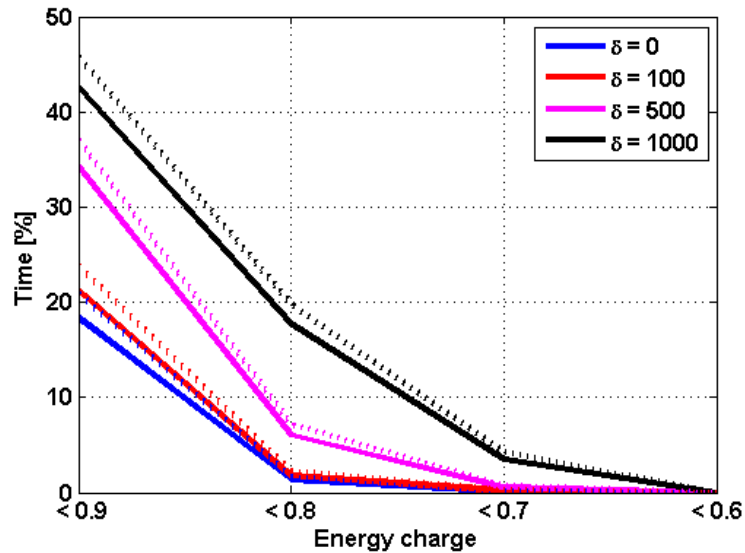


Figure 6.18: Time spent under a certain energy charge level, $\lambda = 0.024$ is represented by the dotted lines and $\lambda = 0.025$ by the solid lines.

6.4 Regulation: $2\lambda - \mu_1 - 2\mu_2 = 0$

Another way to regulate the system, purely theoretical, is to adjust the *Gluc* influx rate λ to a value that satisfies the equation for a stable deterministic system (5.12). This has been done by setting the influx rate according to the metabolic rates, see (6.3).

$$\lambda = \frac{\mu_1 + 2\mu_2}{2}. \quad (6.3)$$

A time delay δ between the actual change of the influx parameter has also been implemented. Without a time delay the deterministic system is stable if the influx does not exceed 0.055. According to (5.12), this does not occur when:

$$\mu_1 + 2\mu_2 \leq 1.1 \quad (6.4)$$

Results of a simulation with the deterministic system with a time delay of 1500 time units is presented in Figure 6.19. Initial influx rate is zero and metabolic rates are respectively $\mu_1 = 0.02$ and $\mu_2 = 0.02$. It can be seen that initially the energy charge decreases. When the generator receives the systems ideal influx rate, it takes some time for the molecules to get through the first part of the glycolysis pathway and convert *ADP* to *ATP*. At that time the system is stable and the adenylate concentrations and energy charge will stay at the same level.

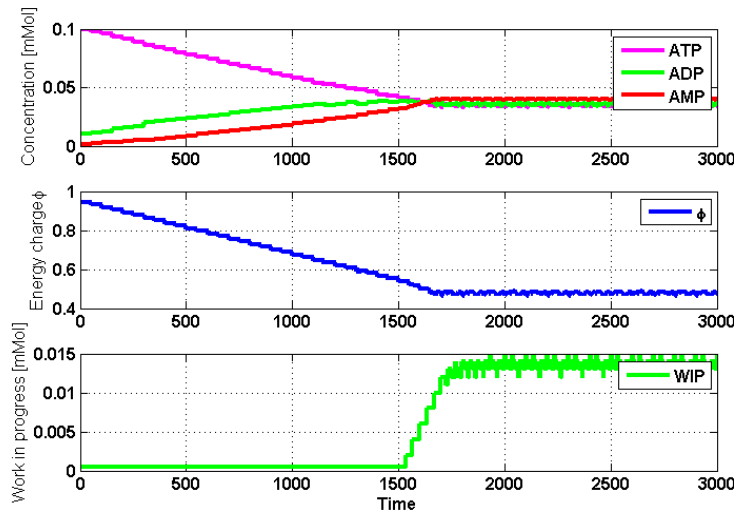


Figure 6.19: $\delta = 1500$, $\mu_1 = 0.02$, $\mu_2 = 0.02$, $\lambda_0 = 0.0$, Deterministic system

In order to get the energy charge back to the desired level, regulation by energy charge is added to the system. Figure 6.20 presents the DEM of the system, process *L* calculates desired influx rate and sends this to generator *G* and energy charge process ϕ gives feedback to make a three-way switch of the generator.

In Figure 6.21 simulation results of this system are presented. The time delay of *L* and the time delay of the energy charge regulator are assumed similar. Metabolic rates are $\mu_1 = 0.01$ and $\mu_2 = 0.01$, there is no initial influx and the time delay is 500. After 500 time units, the influx rate is set. Energy charge stabilizes at 750 time units. The influx increases after 900 time units since the energy charge dropped below 0.90 after 400 time units. This brings the energy charge back to the desired level and it stays there.

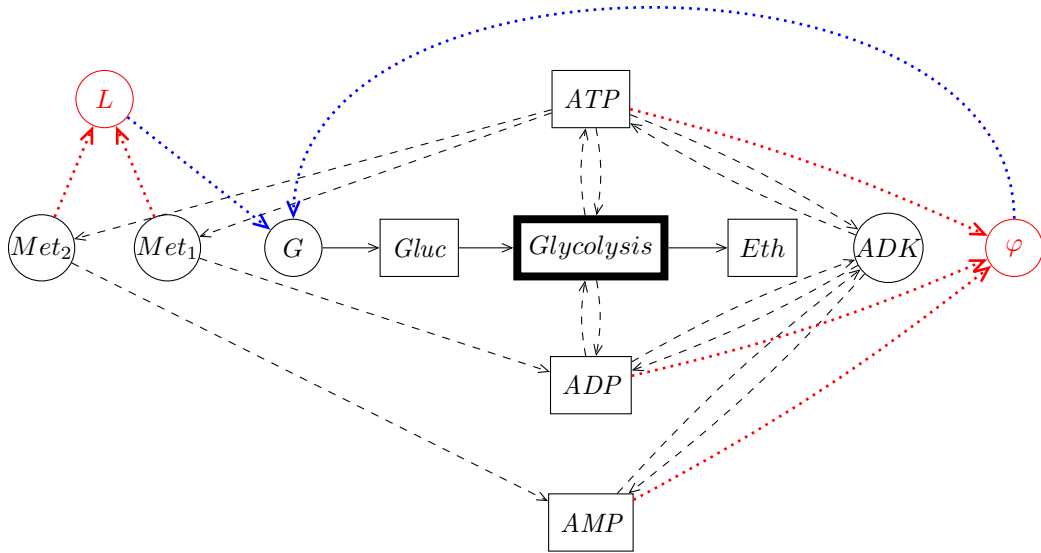


Figure 6.20: DEM representation

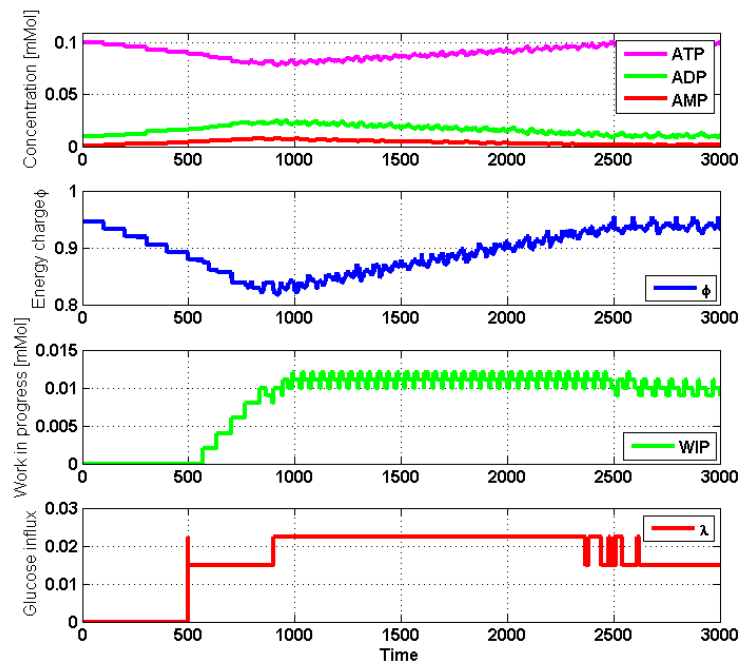


Figure 6.21: $\delta = 500$, $\mu_1 = 0.01$, $\mu_2 = 0.01$, $\lambda_0 = 0.0$, Deterministic system

This system always gives the best possible result with the three-way switch regulator.

6.5 Continuous regulator

In order to increase the *Gluc* influx, glucose receptors are placed in the membrane and glucose influx is lowered by internalizing receptors. In the previous sections we assumed a 3-way switch for the *Gluc* influx rate. Actually, the rate of placing new receptors on the membrane depends on the energy charge level and the receptors internalize at a constant rate, see Figure 6.23. At an energy charge level of 0.95 the placement and internalizing rates are equal, referring to a constant influx. If φ exceeds this threshold, more receptors are internalized than placed and the influx decreases. Below the equilibrium, more receptors are placed than internalized and the influx increases. If the energy charge reaches 0.70, the cell starts to die and therefore no new receptors are placed.

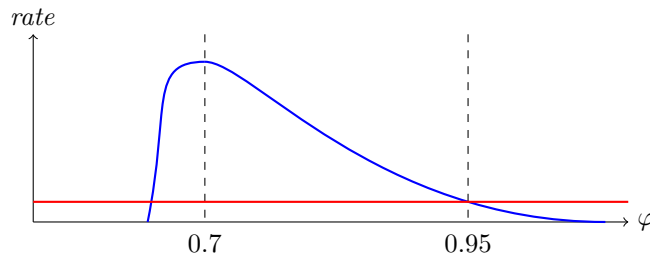


Figure 6.22: Glycolysis receptor decay rate (red) and placement rate (blue).

A first approximation to this continuous glucose influx regulator is to consider it as a linear relation:

$$\lambda = \begin{cases} \lambda + k \cdot (0.95 - \varphi) & \text{if } \varphi \geq 0.70 \\ 0.0 & \text{if } \varphi < 0.70 \end{cases} \quad (6.5)$$

with k a rate constant determining the slope. Since φ changes a lot, a sampling time δ_s has been introduced. The mean energy charge level is calculated over this time period and the influx is updated every δ_s time units. Figure 6.23 shows a graphical representation of this regulator. Results of the system with the linear regulator are presented in Figure 6.24.

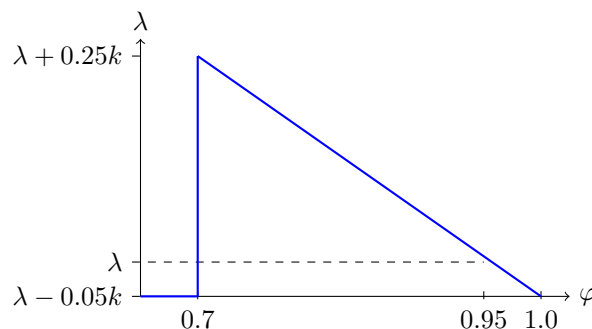


Figure 6.23: Linear glucose update.

It can be seen that the feedback results in a diverging periodic oscillation in the influx rate. This is caused by the time delay between change in influx and the corresponding change in energy charge. It takes about 200 time units for the effect of changing the influx rate can be noticed in the energy charge level. An increase in parameter k increases the

steepness and therefore also shortens the period of the change in influx and an increase in δ_s decreases the steepness and therefore also decreases the period, see Figure 6.25.

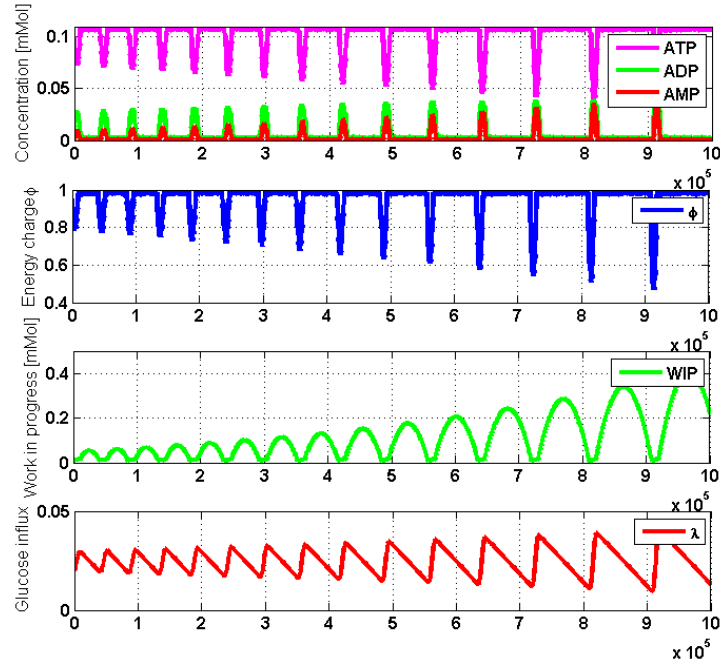


Figure 6.24: $\mu_1 = 0.015$, $\mu_2 = 0.017$, $\lambda_0 = 0.02$, $k = 1e^{-4}$ and $\delta_s = 100$ time units

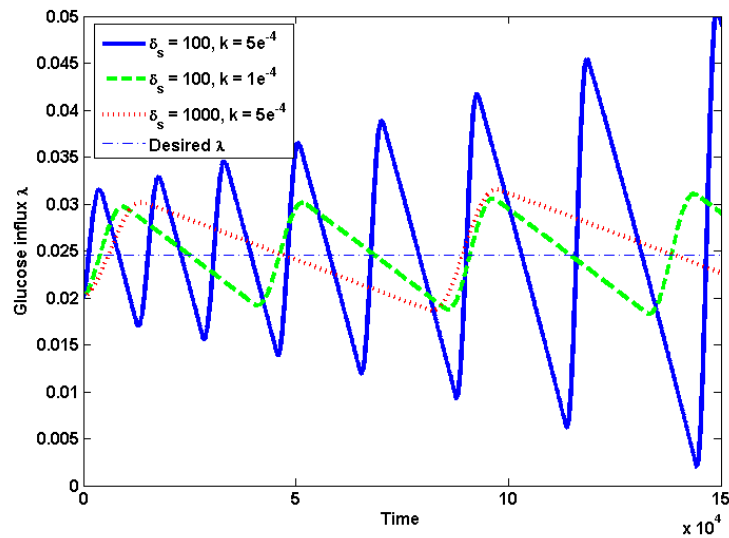


Figure 6.25: $\mu_1 = 0.015$, $\mu_2 = 0.017$, $\lambda_0 = 0.02$ and different values of k and δ_s

Another option is to use a quadratic relation, presented in 6.6. This relation results in a very small increase or decrease in the influx if the energy charge is near the desired level and a large change if the energy charge is far from the desired level. Results of simulations with this system are presented in Figure 6.26. The influx does not converge to the desired rate, but shows the same response as for the linear model.

$$\lambda = \begin{cases} \lambda + k \cdot (0.95 - \varphi)^2 & \text{if } \varphi \leq 0.95 \\ \lambda - k \cdot (0.95 - \varphi)^2 & \text{if } \varphi > 0.95 \end{cases} \quad (6.6)$$

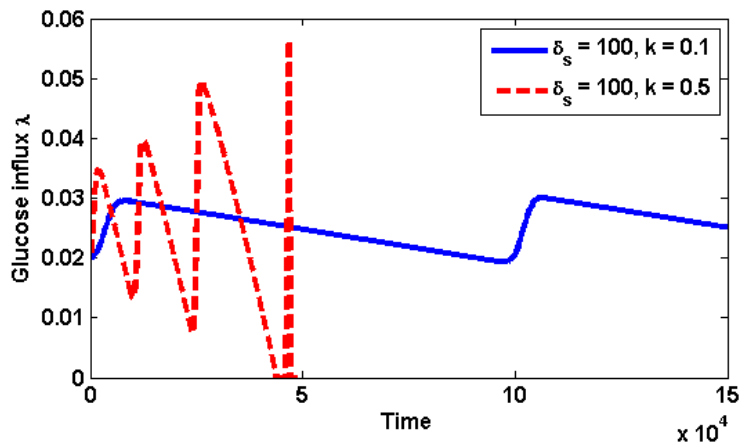


Figure 6.26: $\mu_1 = 0.015$, $\mu_2 = 0.017$, $\lambda_0 = 0.02$ and different values of k and δ_s

As it can be seen, these continuous regulators do not perform well. This is an interesting topic of further research.

6.6 Conclusions

With a feedback loop from the energy charge to the glucose influx and a simple three-way switch the energy balance system can be stabilized and the region of stable input parameters has been expanded. But, enzymes cannot sense the energy charge: the reactions they catalyze depend on molecule concentrations. It is not precisely clear how the cells maintain the energy charge level but this direct feedback results in a stable energy balance system, with the overall energy charge close to the desired level. However, with stochastic distributions the energy charge starts fluctuating and ultimately causes the cell to die. Another approach was implementing enzyme *AMPH* as regulator, depending on the *ATP/AMP* ratio. This also resulted in a stable system, with overall energy charge at the desired level. The *AMPK* regulated system has a higher overall energy charge but with stochastic distributions cells die a little earlier compared to the energy charge regulated system. A third regulator, based on the ideal relation between influx and metabolic rates, also resulted in a stable system. Finally some steps towards a continuous influx regulator have been presented.

Chapter 7

Conclusions and recommendations

This report is an elaboration of the work in [14] and presents the modeling of a substrate-enzyme network as a discrete event model (DEM). The glycolysis pathway is chosen as the network and first modeled as a set of ODEs. The DEM has been constructed out of four different types of reactions; single substrate-enzyme reactions, bi-substrate enzyme reactions, reversible reactions and reactions with down- and upstream inhibiting or activating feedback. This DEM without the feedback reactions has been verified by the set of ODEs.

Deterministic and stochastic behavior of the transient system with a low number of molecules has been investigated. For lots of molecules the results of the deterministic and stochastic behavior are almost similar. In this case an ODE model would be the best choice as a model since it is computationally less expensive. The difference between the stochastic and deterministic model become significant when there are few molecules in the system. The mean clearing time of the results with the stochastic system is almost similar to the deterministic results, what is unthinkable regarding the pathway as a manufacturing line consisting of 12 machines and buffers in between. However, the difference in clearing times is pretty large. This system can not be compared to a usual manufacturing line because the mean search time depends on the number of products in the buffer.

With a convertor between the *ADP* and *ATP* the system has been extended to a steady-state system. Given the stochastic DEM a boundary analysis has been conducted. Three regimes can be distinguished; one stable regime and three unstable regimes. The unstable regimes result in no throughput due to a high demand for *ATP*, or less output than input due to a low demand for *ATP*. The system is only stable if the conversion rate is twice the arrival rate.

In order to keep the energy molecule concentrations balanced and to remove the convertor metabolic reactions and an energy-molecule equilibrating enzyme have been added to the glycolysis pathway. The term 'energy charge' has been introduced to have a measure of the energy-molecule ratio. Expanding the system with the metabolic reactions and extra enzyme was thought to stabilize the system and to be robust, but only for a specific relation between input and metabolic rate parameters the deterministic system is proven stable. Furthermore, using stochastic distributions, the system can't be stabilized.

To stabilize the energy balance system, feedback regulators based on energy charge, *ATP/AMP*-ratio and a regulator based on the metabolic rates have been introduced. These regulators act as a three-way switch and all increase the robustness and area of input parameters for a stable deterministic and stochastic system. The stochastic influence on the system is clearly noticeable by looking at the energy charge. Where it in the deterministic setting remains closely at a value of 0.95, the stochastic results show a large fluctuation between 1.0 and 0.65. This is an important feature since the energy molecules in the cell are necessary for its activity and to keep the membrane at its place. If the energy charge level drops below 0.70, it is believed to be too low for the cell to maintain its membrane and causes the cell to die.

As suggestions for further work, one could look into implementing a PID-regulator in the energy balance system to see if it stabilizes the system better. Since there is a time delay between *Gluc* influx and change in energy charge, a feedback with time delay is also an option.

In order to compare the performance of this system with experiments, the number of enzymes have to be matched. In this report, we assumed all enzymes in the system to have the same mass, which is in contrast with the real situation.

These building blocks for networks of substrate-enzyme reactions can be used to construct other networks, such as signal transducing pathways.

Bibliography

- [1] Bruce Alberts, Alexander Johnson, Julian Lewis, Martin Raff, Keith Roberts, and Peter Walter. *Molecular Biology of the Cell, Fifth Edition*. Garland, 2008.
- [2] D. E. Atkinson. *Cellular Energy Metabolism and Its Regulation*. New York Academic Press, 1977.
- [3] A.G. Chapman, L. Fall, and D.E. Atkinson. Adenylate Energy Charge in Escherichia coli During Growth and Starvation. *J Bacteriol.*, 108(3):1072-1086, December 1971.
- [4] C. Chase and P.J. Ramadge. On real-time scheduling policies for flexible manufacturing systems. *Automatic Control, IEEE Transactions on*, 37(4):491-496, Apr 1992.
- [5] Rene J. Dubos and Thomas D. Brock. *Pasteur and modern science*. Science Tech Publishers ; Springer-Verlag, Madison, WI ; Berlin ; New York, new illustrated ed. edition, 1995.
- [6] P. Dzeja and A. Terzic. Adenylate Kinase and AMP Signaling Networks: Metabolic Monitoring, Signal Communication and Body Energy Sensing. *International Journal of Molecular Sciences*, 10(4):1729-1772, 2009.
- [7] D.G. Hardie, J.W. Scott, D.A. Pan, and E.R Hudson. Management of cellular energy by the AMP-activated protein kinase system. *FEBS Letters*, 546(1):113-120, 2003.
- [8] Nobu Ishiia and Yoshi Sugaa. Dynamic simulation of an in vitro multi-enzyme system. *FEBS Letters*, 581(3):413-420, December 2007.
- [9] N. Kresge, R.D. Simoni, and R.L. Hill. Otto Fritz Meyerhof and the Elucidation of the Glycolytic Pathway. *The Journal of Biological Chemistry*, 280(4), January 2005.
- [10] J.E. Rooda and J. Vervoort. *Analysis of manufacturing systems*. Eindhoven University of Technology, Systems Engineering Group, Department of Mechanical Engineering, Eindhoven, The Netherlands, 2007.
- [11] B. Teusink, J. Passarge, C. A. Reijenga, E. Esgalhado, C. C. van der Weijden, M. Schepper, M. C. Walsh, B. M. Bakker, K. van Dam, H. V. Westerhoff, and J. L. Snoep. Can yeast glycolysis be understood in terms of in vitro kinetics of the constituent enzymes? Testing biochemistry. *Eur J Biochem*, 267(17):5313-5329, September 2000.
- [12] E. A. F. van de Rijt. Discrete event simulations for biological systems. Master's thesis, Systems Engineering Group, Department of Mechanical Engineering, Eindhoven, The Netherlands, 2008.
- [13] Wikipedia. Glycolysis.
- [14] D.A.J. van Zwieten, J.E. Rooda, D. Armbruster, and J.D. Nagy. Feedback and reversibility in substrate-enzyme reactions as discrete event models. SE Report 2010-01, Eindhoven University of Technology, Systems Engineering Group, Department of Mechanical Engineering, Eindhoven, The Netherlands, 2010.

Appendix A

Parameters

Table A.1: Parameters for the glycolysis pathway [11].

Enzyme	Scaled v_{\max}	K_s	K_s energy	K_{eq}	type
HK	0.089	0.08	0.15		bi-substrate
PGI	0.134	1.4	0.3	0.314	reversible
PFK	0.0723	0.1	0.71		bi-substrate
Ald	0.127	0.3			substrate
TPI	0.894	0.02^1			substrate
GAPDH	0.468	0.21	0.09		bi-substrate
PGK	0.511	0.003	0.2		bi-substrate
PGM	1.00	1.2	0.1	0.19	reversible
Eno	0.144	0.04			substrate
PYK	0.431	0.14	0.53		bi-substrate
PDC	0.0691	4.33			substrate
ADH	0.319	1.11	0.031		bi-substrate
ADK	5.0^2	0.001^2	0.001^2		
Met	$1.0 - 10.0^3$				

¹ Unknown parameter, assumption.

² Unknown parameter, assumption. Very fast reaction.

³ Metabolism rate.

Appendix B

Chi processes

For the glycolysis cycle and adenylate transitions some new processes must be defined.

B.1 Enzymes

B.1.1 One substrate molecule in, two product molecules out *E12*

This process is almost similar to the basic enzyme with one molecule, but it has got two product molecules, see Figure B.1.

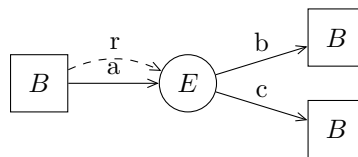


Figure B.1: DEM representation of process *E12*.

Chi file:

```
proc E12( chan a?,b!,c!: mol, r?: nat, val Vmax, km, tr: real ) =
| [ chan q: void
  , var x: mol
    , tStart, tp, ts: real
    , concS: nat = 0
    , search, rec: bool = ( false, false )
  :: *( concS > 0 -> tStart := time
    ; search:= true
    ; search
```



```

    *> ( ts := ( tStart + meanST( km, tr, concS )
              - time ) max 0.0
        ;( delay ts; rec:= true; search:= false
          | q?
            ; ( concS > 0 -> skip
              | concS = 0 -> rec:= false; search:= false
              )
            )
          )
        ; ( rec -> a?x
          ; tp:= 1 / Vmax
          ; delay tp
          ; b!x; c!x
          | not rec -> skip
          )
        )
  || *( r?concS; ( search -> q!
                | not search -> skip
                )
      )
  ]|

```

Model input:

```
proc E12( a?, b!, c!, r?, Vmax, km, tr )
```

B.1.2 Reversible one in, two out ($E12_R$)

This enzyme can receive and send molecules to three different buffers and also communicates with these buffers, like enzyme *ADK*, see Figure B.2. The conversion direction, according to (5.7), is determined by:

$$\begin{cases} 2ADP \rightarrow ATP + AMP & \text{if } ([ATP] + 1) \cdot ([AMP] + 1) \leq ([ADP] - 2)^2 \\ ATP + AMP \rightarrow 2ADP & \text{if } ([ATP] - 1) \cdot ([AMP] - 1) \geq ([ADP] + 2)^2 \end{cases} \quad (\text{B.1})$$

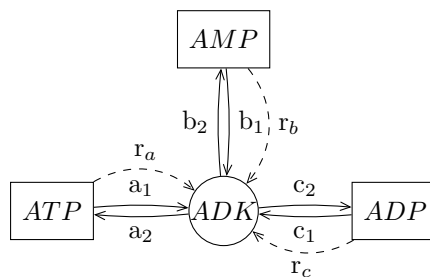


Figure B.2: DEM representation of enzyme *ADK*.

Chi file:

```
proc E12R( chan a1?,a2!,b1?,b2!,c1?,c2!: mol, ra?,rb?,rc?: nat
```

```

        , val Vmax,km,km1,km2,tr,n: real
    ) =
[[ chan q: void
  , var x1,x2: mol
    , tStart, ts, tp : real
    , ca,cb,cc: nat = ( 0, 0, 0 )
    , cA,cB,cC: real = ( 0.0, 0.0, 0.0 )
    , search,rec,sin: bool = ( false, false, false )
  :: *( ( (cA-1) * (cB-1) >= (cC+2)^2 -> sin:= false
    | (cA+1) * (cB+1) <= (cC-2)^2 -> sin:= true
    )
    ; tStart := time
    ; search:= true
    ; search
    * > ( ( not sin -> ts:= ( tStart + meanST1(km1,km2,tr,n,ca,cb) - time ) max 0.0
      | sin -> ts:= ( tStart + meanST( km, tr, cc ) - time ) max 0.0
      )
      ;( delay ts; rec:= true; search:= false
      | q?
        ; ( sin and (cA-1) * (cB-1) >= (cC+2)^2 -> skip
          | sin and (cA-1) * (cB-1) < (cC+2)^2 -> rec:= false; search:= false
          | not sin and (cA+1) * (cB+1) <= (cC-2)^2 -> skip
          | not sin and (cA+1) * (cB+1) > (cC-2)^2 -> rec:= false; search:= false
          )
        )
      )
    ;( rec and sin -> c1?x1; c1?x2
      ; tp:= 1 / Vmax
      ; delay tp
      ; a2!x1; b2!x2
      | rec and not sin -> a1?x1; b1?x2
      ; tp:= 1 / Vmax
      ; delay tp
      ; c2!x1; c2!x2
      | not rec -> skip
      )
    )
  || *(( ra?ca; cA:=n2r(ca) | rb?cb; cB:=n2r(cb) | rc?cc; cC:=n2r(cc) )
    ; ( search -> q!
      | not search -> skip
      )
    )
  ]]
```

Model input:

```
proc E12R( a1?,a2!,b1?,b2!,c1?,c2,ra?,rb?,rc?,Vmax,km,km1,km2,tr,n )
```

B.2 Metabolism

Metabolism can be modeled as a drain on the *ATP*-buffer with a certain drain rate, or as an enzyme with the *ATP* conversion to *ADP* or *AMP* depending on the *ATP* concentration.

B.2.1 Drain *D12P*

When metabolism is considered as a simple drain, it takes *ATP* molecules from the buffer at a fixed rate and reconfigures them into *ADP* and *AMP*, see Figure B.3, by taking a sample out of a uniform distribution and comparing it to the fraction of *ADP* products.

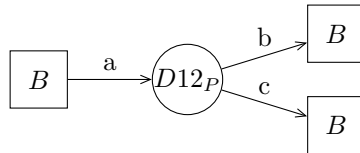


Figure B.3: DEM representation of process *D12P*.

Chi file:

```
proc DP( chan a?,b!,c!: mol, val Vmax, frac1: real ) =
| [ var x: mol, u, at: real
    , uni: -> real = uniform ( 0.0 , 1.0 )
  :: *( a?x; at:= 1/Vmax ; delay at
    ; u:= sample uni
    ; ( u <= frac1 -> b!x
      | u > frac1 -> c!x
    )
  )
] |
```

Model input:

```
proc DP( a?,b!,c!, Vmax, frac1 ) =
```

B.3 Buffers

B.3.1 Buffer with 3 communication channels *B3*

The *ADP* buffer has got two outgoing channels in the glycolysis cycle and with the adenylate transitions an extra channel with communication is required for enzyme *ADK*. The buffer model is presented in Figure B.4. Chi file:

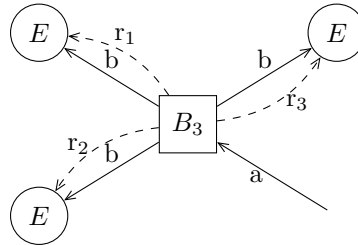


Figure B.4: DEM representation of process B_4c3 .

```

proc B3( chan a?,b!: mol, r1!,r2!,r3!: nat
        , dt!: (string,nat), val S0: nat, id: string
        ) =
[[ var xs: [mol] = []
   , x: mol
   , uni: -> real = uniform ( 0.0 , 1.0 )
   , i: nat = 1
:: i <= S0
 * > ( xs:= injBuff ( xs, (i,time), sample uni ); i:= i + 1 )
; r1!len(xs); r2!len(xs); r3!len(xs)
; *( dt !!( id , len (xs))
    ; ( a?x; xs:= injBuff ( xs, x, sample uni)
      | len (xs) > 0 -> b!hd(xs); xs := tl(xs)
      )
    ; r1!len(xs); r2!len(xs); r3!len(xs)
    )
]]

```

Model input:

```

proc B3( a?,b!,r1!,r2!,r3!,dt!,S0,id ) =

```

B.3.2 Buffer with 4 communication channels B_4

If the *ATP*-dependent metabolism process and enzyme *ADK* is added to the glycolysis model, the *ATP* buffer must have 4 outgoing channels with communication, see Figure B.5. Chi file:

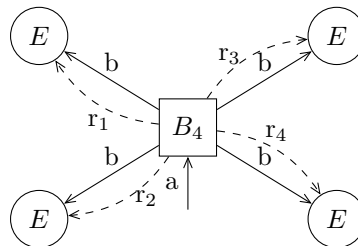


Figure B.5: DEM representation of process B_4 .

```

proc B4( chan a?,b!: mol, r1!,r2!,r3!,r4!: nat
      , dt!: (string,nat), val S0: nat, id: string
      ) =
  |[ var xs: [mol] = []
    , x: mol
    , uni: -> real = uniform ( 0.0 , 1.0 )
    , i: nat = 1
  :: i <= S0
    *> ( xs:= injBuff ( xs, (i,time), sample uni ); i:= i + 1 )
    ; r1!len(xs); r2!len(xs); r3!len(xs); r4!len(xs)
    ; *( dt !!( id , len (xs))
      ; ( a?x; xs:= injBuff ( xs, x, sample uni)
        | len (xs) > 0 -> b!hd(xs); xs := tl(xs)
        )
      ; r1!len(xs); r2!len(xs); r3!len(xs); r4!len(xs)
    )
  ]|

```

Model input:

```

proc B4( a?,b!,r1!,r2!,r3!,r4!,dt!,S0,id ) =

```

Appendix C

Chi models

C.1 Glycolysis pathway

The discrete event model of the glycolysis pathway from Chapter 4 with all communication channels is presented in Figure C.1. The χ code is presented in Table C.2.

Table C.1: EMP pathway model.

Chi code	Reference
<code>type mol = (nat, real) // id, timein</code>	
Process <i>G</i>	[14]
Process <i>B1</i>	[14]
Process <i>B2</i>	[14]
Process <i>BX</i>	[14]
Process <i>E1</i>	[14]
Process <i>E12</i>	(B.1.1)
Process <i>E2</i>	[14]
Process <i>Erev</i>	[14]
Process <i>DT</i>	[14]
Function <i>injBuff</i>	[14]
Function <i>cond</i>	[14]
Function <i>calcVpgiRev</i>	[14]
Function <i>meanST</i>	[14]
Function <i>meanST1</i>	[14]

The model is defined by:

```
model L( val lambdaG: real ) =
| [ chan mg,m1,m2,m3,m3r,m4,m4r,m5,m6,m7,m8,m9,m10,m12,m13,m14,m15
  , m16,m17,m18,m19,m20,m21,m22,m23,m24,m25,m26
```

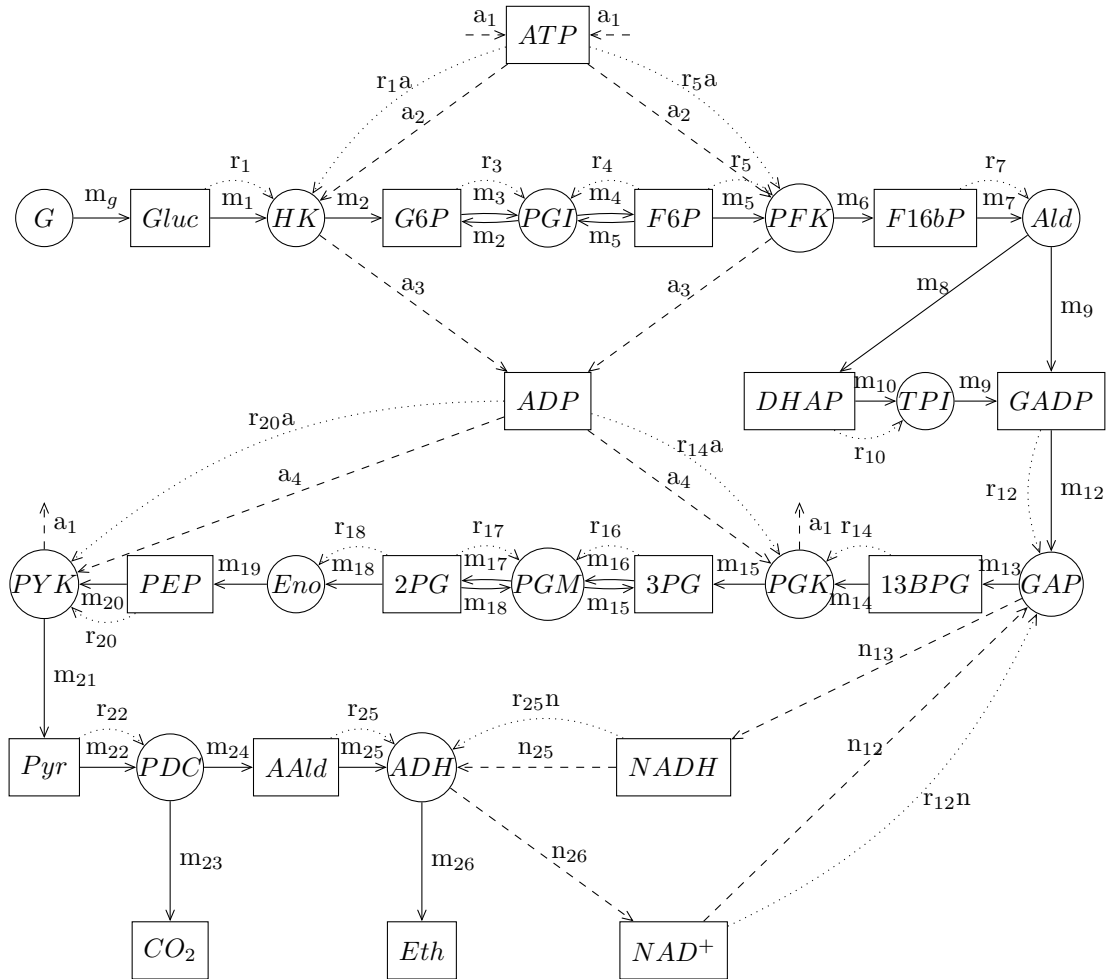


Figure C.1: DEM representation of the glycolysis pathway.

```

, a1,a2,a3,a4,n12,n13,n25,n26: mol
, r1,r1a,r3,r4,r5,r5a,r7,r10,r12n,r14,r14a,r16,r17,r18
, r20,r20a,r22,r25,r25n: nat
, dt: (string , nat)
, var c1, c2, c3, c4, c5, c6, c7, c8, c9, c10, c11, c13: nat
= (3000,3000,3000,3000,3000,3000,3000,3000,3000,3000,3000,3000)
, c15,c16,c17,c18: nat = (5000,5000,5000,5000)
:: DT(dt)
//// G (mg,1/lambdaG)
|| B1 (mg,m1,r1,dt,c1,"Gluc") //b GLUC
|| E2 (m1,m2,a2,a3,r1,r1a
,89.0,80.0,150.0,0.0112359551,1.0) //e HK
|| B1 (m2,m3,r3,dt,c2,"G6P") //b G6P
|| Erev (m3,m4,m5,m2,r3,r4
,134.0,1400.0,300.0,0.314,0.0074626866) //e PGI
|| B2 (m4,m5,r4,r5,dt,c3,"F6P") //b F6P
|| E2 (m5,m6,a2,a3,r5,r5a
,72.3,100.0,710.0,0.0138312586,1.0 ) //e PFK

```

```

|| B1 (m6,m7,r7,dt,c4,"F16bP") //b F16bP
|| E12 (m7,m8,m9,r7,127.0,300.0,0.0078740157 ) //e Ald
|| B1 (m8,m10,r10,dt,c5,"DHAP") //b DHAP
|| E1 (m10,m9,r10,894.0,20.0,0.0011185682 ) //e TPI
|| B1 (m9,m12,r12,dt,c6,"GADP") //b GADP
|| E2 (m12,m13,n12,n13,r12,r12n
,468.0,210.0,90.0,0.0021367521,1.0 ) //e GAPDH
|| B1 (m13,m14,r14,dt,c7,"13bPG") //b 1,3bPG
|| E2 (m14,m15,a4,a1,r14,r14a
,511.0,3.0,200.0,0.0019569472,1.0 ) //e PGK
|| B1 (m15,m16,r16,dt,c8,"3PG") //b 3PG
|| Erev (m16,m17,m18,m15,r16,r17
,1000.0,1200.0,100.0,0.19,0.001) //e PGM
|| B2 (m17,m18,r17,r18,dt,c9,"2PG") //b 2PG
|| E1 (m18,m19,r18,144.0,40.0,0.006944444 ) //e Eno
|| B1 (m19,m20,r20,dt,c10,"PEP") //b PEP
|| E2 (m20,m21,a4,a1,r20,r20a
,431.0,140.0,530.0,0.0023201856,1.0 ) //e PYK
|| B1 (m21,m22,r22,dt,c11,"Pyr") //b Pyr
|| E12 (m22,m23,m24,r22,69.1,4330.0,0.01447178 ) //e Ald
|| BX (m23,dt,"CO2") //b CO2
|| B1 (m24,m25,r25,dt,c13,"AcAld") //b AcAld
|| E2 (m25,m26,n25,n26,r25,r25n
,319.0,1110.0,31.0,0.0031347962,1.0 ) //e ADH
|| BX (m26,dt,"Eth") //b Eth
|| B1 (n13,n25,r25n,dt,c15,"NADH") //b NADH
|| B1 (n26,n12,r12n,dt,c16,"NAD+") //b NAD+
|| B2 (a1,a2,r1a,r5a,dt,c17,"ATP") //b ATP
|| B2 (a3,a4,r14a,r20a,dt,c18,"ADP") //b ADP
]|

```


C.2 Adenylate transitions

In Chapter 5 the glycolysis pathway is extended with adenylate transitions, see Figure C.2

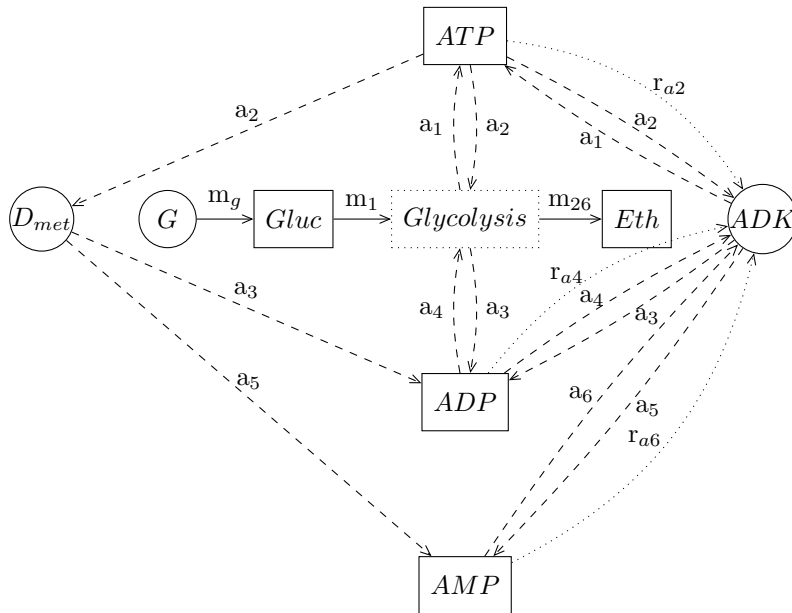


Figure C.2: DEM representation of the glycolysis pathway with adenylate transitions.

Table C.2: EMP pathway model.

Chi code	Reference
<code>type mol = (nat, real) // id, timein</code>	
Process G	[14]
Process $B1$	[14]
Process $B2$	[14]
Process BX	[14]
Process $E1$	[14]
Process $E12$	(B.1.1)
Process $E12R$	(B.1.2)
Process $E2$	[14]
Process $Erev$	[14]
Process $D12$	(B.2.1)
Process DT	[14]
Function $injBuff$	[14]
Function $cond$	[14]
Function $calcVpgiRev$	[14]
Function $meanST$	[14]
Function $meanST1$	[14]

The model is defined by:

```

model L( val lambdaG: real ) =
|[ chan mg,m1,m2,m3,m3r,m4,m4r,m5,m6,m7,m8,m9,m10,m12,m13,m14,m15
  , m16,m17,m18,m19,m20,m21,m22,m23,m24,m25,m26
  , a1,a2,a3,a4,a5,a6,n12,n13,n25,n26: mol
  , r1,r1a,r3,r4,r5,r5a,r7,r10,r12,r12n,r14,r14a,r16,r17,r18
  , r20,r20a,r22,r25,r25n,ra2,ra4,ra6: nat
  , dt: (string , nat)
  , var c1, c2, c3, c4, c5, c6, c7, c8, c9, c10, c11, c13: nat
    = (3000,3000,3000,3000,3000,3000,3000,3000,3000,3000,3000,3000,3000)
  , c15,c16,c17,c18,c19: nat = (5000,5000,5000,5000,5000)
:: DT(dt)
//|| G (mg,1/lambdaG)
|| B1 (mg,m1,r1,dt,c1,"Gluc") //b GLUC
|| E2 (m1,m2,a2,a3,r1,r1a
      ,89.0,80.0,150.0,0.0112359551,1.0) //e HK
|| B1 (m2,m3,r3,dt,c2,"G6P") //b G6P
|| Erev (m3,m4,m5,m2,r3,r4
        ,134.0,1400.0,300.0,0.314,0.0074626866) //e PGI
|| B2 (m4,m5,r4,r5,dt,c3,"F6P") //b F6P
|| E2 (m5,m6,a2,a3,r5,r5a
      ,72.3,100.0,710.0,0.0138312586,1.0 ) //e PFK
|| B1 (m6,m7,r7,dt,c4,"F16bP") //b F16bP
|| E12 (m7,m8,m9,r7,127.0,300.0,0.0078740157 ) //e Ald
|| B1 (m8,m10,r10,dt,c5,"DHAP") //b DHAP
|| E1 (m10,m9,r10,894.0,20.0,0.0011185682 ) //e TPI
|| B1 (m9,m12,r12,dt,c6,"GADP") //b GADP
|| E2 (m12,m13,n12,n13,r12,r12n
      ,468.0,210.0,90.0,0.0021367521,1.0 ) //e GAPDH
|| B1 (m13,m14,r14,dt,c7,"13bPG") //b 1,3bPG
|| E2 (m14,m15,a4,a1,r14,r14a
      ,511.0,3.0,200.0,0.0019569472,1.0 ) //e PGK
|| B1 (m15,m16,r16,dt,c8,"3PG") //b 3PG
|| Erev (m16,m17,m18,m15,r16,r17
        ,1000.0,1200.0,100.0,0.19,0.001) //e PGM
|| B2 (m17,m18,r17,r18,dt,c9,"2PG") //b 2PG
|| E1 (m18,m19,r18,144.0,40.0,0.006944444 ) //e Eno
|| B1 (m19,m20,r20,dt,c10,"PEP") //b PEP
|| E2 (m20,m21,a4,a1,r20,r20a
      ,431.0,140.0,530.0,0.0023201856,1.0 ) //e PYK
|| B1 (m21,m22,r22,dt,c11,"Pyr") //b Pyr
|| E12 (m22,m23,m24,r22,69.1,4330.0,0.01447178 ) //e Ald
|| BX (m23,dt,"CO2") //b CO2
|| B1 (m24,m25,r25,dt,c13,"AcAld") //b AcAld
|| E2 (m25,m26,n25,n26,r25,r25n
      ,319.0,1110.0,31.0,0.0031347962,1.0 ) //e ADH
|| BX (m26,dt,"Eth") //b Eth
|| B1 (n13,n25,r25n,dt,c15,"NADH") //b NADH
|| B1 (n26,n12,r12n,dt,c16,"NAD+") //b NAD+
|| B3 (a1,a2,r1a,r5a,ra2,dt,c17,"ATP") //b ATP
|| B3 (a3,a4,r14a,r20a,ra4,dt,c18,"ADP") //b ADP
|| B1 (a5,a6,ra6,dt,c19,"AMP") //b AMP
|| DP (a2,a3,a5,1000.0,0.8) //D Metabolism drain (rest)
|| E12R (a2,a1,a6,a5,a4,a3,ra2,ra6,ra4
        ,5000.0,1.0,1.0,1.0,0.0002,1.0) //e ADK
]|

```